JCI The Journal of Clinical Investigation

C5aR1 signaling triggers lung immunopathology in COVID-19 through neutrophil extracellular traps

Bruna M.S. Silva, … , Paul Proost, Thiago M. Cunha

J Clin Invest. 2023. https://doi.org/10.1172/JCI163105.

Research In-Press Preview Inflammation

Graphical abstract

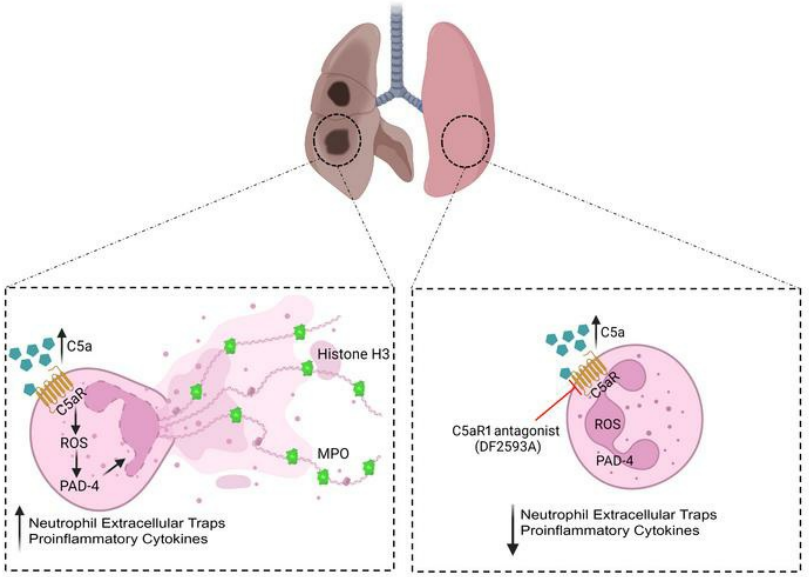

Find the latest version:

https://jci.me/163105/pdf

C5aR1 signaling triggers lung immunopathology in COVID-19 through neutrophil extracellular traps

Bruna M. Silva[1,2#], Giovanni F. Gomes[1#], Flavio P. Veras[1#], Seppe Cambier[3], Gabriel V. L. Silva[1,2], Andreza U. Quadros[1], Diego B. Caetité[1,2], Daniele C. Nascimento[1,2], Camilla M. Silva[1,2], Juliana C. Silva[1], Samara Damasceno[1], Ayda H. Schneider [1], Fabio Beretta[3], Sabrina S. Batah[4], Icaro M. S. Castro[5], Isadora M. Paiva[1], Tamara Rodrigues[1,2], Ana Salina[1,6], Ronaldo Martins[6,7], Guilherme C.M. Cebinelli[1,2], Naira L. Bibo[1], Daniel M. Jorge[6,7], Helder I. Nakaya[5], Dario S. Zamboni[1,6], Luiz O. Leiria[1,2], Alexandre T. Fabro[4], José C. Alves-Filho[1,2], Eurico Arruda[6,7], Paulo Louzada-Junior[1,8], Renê D. Oliveira[1,8], Larissa D. Cunha[1,6], Pierre Van Mol[9], Lore Vanderbeke[10], Simon Feys[10], Els Wauters[9], Laura Brandolini[11], Andrea Aramini[11] Fernando Q. Cunha[1,2], Jörg Köhl[12,13], Marcello Allegretti[11], Diether Lambrechts[14], Joost Wauters[10,15], Paul Proost[3], Thiago M. Cunha[1,2]*

[1]Center for Research in Inflammatory Diseases (CRID), Department of Pharmacology, Ribeirão Preto Medical School, University of São Paulo, Ribeirão Preto, São Paulo, Brazil; [2]Graduate Program in Basic and Apply Immunology, Ribeirão Preto Medical School, University of São Paulo, Ribeirão Preto, São Paulo, Brazil; [3] Laboratory of Molecular Immunology, Department of Microbiology, Immunology and Transplantation, Rega Institute, KU Leuven, Leuven, Belgium. [4]Department of Pathology and Legal Medicine, Ribeirão Preto Medical School, University of São Paulo, Ribeirão Preto, São Paulo, Brazil; [5] Hospital Israelita Albert Einstein, São Paulo, Brazil; [6]Department of Cell and Molecular Biology, Ribeirão Preto Medical School, University of São Paulo, Ribeirão Preto, São Paulo, Brazil; [7] Virology Research Center, Ribeirão Preto Medical School, University of São Paulo, Ribeirão Preto, São Paulo, Brazil; [8]Divisions of Clinical Immunology, Emergency, Infectious Diseases and Intensive Care Unit, Ribeirão Preto Medical School, University of São Paulo, Ribeirão Preto, São Paulo, Brazil; [9] Laboratory of Respiratory Diseases and Thoracic Surgery (BREATHE), Department of Chronic Diseases and Metabolism, KU Leuven, Leuven, Belgium; [10]Laboratory for Clinical Infectious and Inflammatory Disorders, Department of Microbiology, Immunology and Transplantation, KU Leuven, Leuven, Belgium; [11] R&D Department, Dompé Farmaceutici s.p.a., via Campo di Pile, 67100 L'Aquila, Italy; [12]Pain Research Center, Department of Anesthesiology, University of Cincinnati College of Medicine, Cincinnati, Ohio, 45267, USA; [13]Institute for Systemic Inflammation Research, University of Lübeck, Ratzebuger Allee 160 23562 Lübeck, Germany; [14]Laboratory of Translational Genetics, Department of Human Genetics, VIB-KU Leuven, Leuven, Belgium; [15] Medical Intensive Care Unit, University Hospitals Leuven, 3000 Leuven, Belgium.

[#] Contributed equally

*Correspondence should be addressed: Thiago M. Cunha; Ribeirao Preto Medical School – USP, Avenida Bandeirantes, 3900, 14049-900, Ribeirao Preto, SP, Brazil. Tel: +55 16 3315-0199; E-mail for contact: thicunha@fmrp.usp.br

Short Title: C5aR1-signaling mediates COVID-19 immunopathology

Abstract

Patients with severe COVID-19 develop acute respiratory distress syndrome (ARDS) that may progress to cytokine storm syndrome, organ dysfunction, and death. Considering that complement component 5a (C5a), through its cellular receptor C5aR1, has potent proinflammatory actions, and plays immunopathological roles in inflammatory diseases, we investigated whether the C5a/C5aR1 pathway could be involved in COVID-19 pathophysiology. C5a/C5aR1 signaling increased locally in the lung, especially in neutrophils of critically ill COVID-19 patients compared to patients with influenza infection, as well as in the lung tissue of K18-hACE2 Tg mice (Tg mice) infected with SARS-CoV-2. Genetic and pharmacological inhibition of C5aR1 signaling ameliorated lung immunopathology in Tg-infected mice. Mechanistically, we found that C5aR1 signaling drives neutrophil extracellular trap (NET)s-dependent immunopathology. These data confirm the immunopathological role of C5a/C5aR1 signaling in COVID-19 and indicate that antagonists of C5aR1 could be useful for COVID-19 treatment.

Keywords: COVID-19, C5aR1, C5a, SARS-CoV-2, Myeloid cells, Neutrophils, NETs

Introduction

COVID-19 is the major acute global public health issue in this century. Patients with severe COVID-19 develop acute respiratory distress syndrome (ARDS) that may progress to organ dysfunction, and death (1, 2). The disease itself is a consequence of infection with the SARS-CoV-2 virus, which triggers an inflammatory response by the host organism, potentially resulting in a maladaptive inflammatory response and progression to severe disease (3, 4). As in many other human viral diseases, pathology is thus mainly a consequence of the host's response to the virus rather than of the virus itself. Reducing viral loads after the dysfunctional immune response developed may be considered but could be a less favorable therapeutic option compared to appropriate control of inflammation. Combining antiviral with immune control, including the development of specific anti-inflammatory agents to block virus-triggered inflammatory responses, might be a strategic option to treat short-living virus-caused pathology, especially in COVID-19. This hypothesis has been confirmed by the demonstration that drugs targeting the inflammatory response are, at least in part, effective to control COVID-19 severity (5–10). Nevertheless, these therapies need to be used with caution since they may also affect the host immune response against the virus and against secondary/opportunistic infections. Noteworthy, the development of novel agents to treat COVID-19 targeting the inflammatory/immune response should be focused on a mediator/process that is important for immune pathology but dispensable for infection control (11, 12). One possible candidate might be the complement C5a/C5aR1 signaling (11, 12).

C5a is one of the most important components of the complement cascade and possesses several pro-inflammatory actions (13, 14). C5a is a common component of the activation of all complement pathways and acts mainly via the G protein-coupled receptor (GPCR) C5a Receptor type 1 (C5aR1), also called CD88 (14). C5aR1 was initially identified in neutrophils, monocytes/macrophages, and mast cells (14, 15). The C5aR1 signaling has been implicated in the pathophysiology of several inflammatory diseases including virus-infection-induced diseases that cause lung pathology (16–19). For instance, C5a/C5aR1 inhibition alleviates lung damage in murine models of influenza A, Middle East respiratory syndrome coronavirus (MERS-CoV), and respiratory syncytial virus (RSV) (20–22).

A growing body of evidence suggests the possible participation of the complement system, and especially of C5a/C5aR1 signaling in COVID-19 pathophysiology (23, 24).

C5a levels increased in the blood of COVID-19 patients and correlated with disease severity (23). More recent clinical studies have shown a beneficial effect of anti-C5a therapies for COVID-19 (25–27), including a multicenter, double blind, randomized, placebo-controlled, phase 3 clinical trial (28). Nevertheless, no study investigated in depth the outcome of the lack or blockade of C5aR1 signaling on COVID-19, or the mechanisms behind its role. Herein, we found that C5a/C5aR1 signaling is increased in patients and in a preclinical mice model of COVID-19. Furthermore, we show that genetic and pharmacological blockage of C5aR1 signaling in myeloid cells (especially neutrophils) ameliorates COVID-19 lung immunopathology. Finally, we found that the C5aR1 signaling mediates COVID-19 immunopathology through enhancement of neutrophil extracellular traps (NETs) formation.

Results

C5a/C5aR1 signaling in the lung cells of COVID-19 patients

In order to investigate the role of C5a/C5aR1 signaling for the pathophysiology of COVID-19, initially we assessed bronchoalveolar lavage (BAL) fluid from critically ill COVID-19 patients requiring invasive mechanical ventilation, which we have previously reported to contain increased numbers of hyperactivated degranulating neutrophils and elevated concentrations of pro-inflammatory cytokines/chemokines (e.g. IL-1β, G-CSF, CXCL1 and CXCL8) compared to mechanically ventilated patients with influenza infection as a non–COVID-19 viral pneumonia cohort (29). We analyzed the levels of C5a in these cohorts of patient samples and found significantly higher C5a concentrations in the BAL fluid from COVID-19 patients as compared to influenza-infected patients (Figure 1A). Notably, the levels of factor Bb, but not of C3a, were higher in the BAL fluid from COVID-19 patients as compared to influenza patients (Figure 1, B and C). In addition, the levels of C5a and factor Bb were higher in the BAL fluid compared to the corresponding paired plasma samples in COVID-19 patients (Figure 1, D and E). Together, these results indicate that high C5a levels are produced locally (in lungs) in COVID-19, probably by the activation of alternative complement pathways, and correspond to stronger local complement activation in COVID-19 compared to other severe viral lung infections.

The increased levels of C5a in the BAL fluid might indicate the activation of C5a-C5aR1 signaling. Thus, in an attempt to gain information about the possible role of C5a in the pathophysiology of COVID-19, we sought to identify the possible cell subtype in the

BAL fluid of COVID-19 patients expressing *C5AR1*, its main pro-inflammatory receptor (17, 30). To this end, we assessed our previously published database containing single-cell transcriptomes of BAL fluid cells from COVID-19 and non-COVID-19 pneumonia patients and re-analyzed these data (31). We have found in our re-analyses (Figure 1F) that, among the different clusters of cells, in both groups the expression of *C5AR1* was detected mainly in the neutrophil and monocytes/macrophages populations, and to a limited extend in conventional dendritic cells (cDC) (Figure 1, F - I). In addition, the number of *C5AR1*-expressing neutrophils was higher in the BAL fluid from COVID-19 patients compared to BAL fluid from non-COVID-19 pneumonia patients (Figure 1J). No differences were observed in the number of *C5AR1*-expressing monocytes/macrophages and cDC in these groups (Figure 1J). Notably, the average expression of *C5AR1* per cell of the BAL fluid is similar in both COVID-19 and non-COVID-19 pneumonia patients (Figure 1K). The re-analyses of single-cell transcriptomics did not reveal the significant expression of C5 in the lung cells that was reported before (32) (Supplementary Figure 1), indicating that the increased levels of C5a could be mostly derived from hepatic origin.

A similar result related to the expression of *C5AR1* was revealed by the re-analyses of another public dataset of the single-cell transcriptome of cells from BAL fluid of COVID-19 patients (33), corroborating that *C5AR1*-expressing neutrophils are increased in the lung of COVID-19 patients (Supplementary Figure 2**)**. Of note, this single-cell transcriptome data set also revealed some degree of expression of *C5AR1* in epithelial cells of the BAL fluid of COVID-19 patients (Supplementary Figure 2D).

In order to validate the single-cell transcriptome data, lung tissue from post-mortem COVID-19 patients was used for C5aR1 immunostaining and co-staining for neutrophil (neutrophil elastase; NE) and macrophage/monocyte (Iba-1) cellular markers. In agreement with the single-cell transcriptome, we found that C5aR1 is mainly expressed in NE^+ cells (neutrophils; 41.87 ± 12.77 %; Figure 1, I and J, and Supplementary Figure 4) and Iba-1^+ cells (macrophage/monocytes, 40.87 ± 10.22 %, Figure 2, A and B, and Supplementary Figure 3). The remaining non-identified cells were 17.49 ± 15.52 % (Figure 1B), which could be related to the epithelial cells that we found expressing *C5AR1* in the single-cell transcriptome analyses. Together, these data indicate that, in COVID-19, the enhanced production of C5a in the lung is mainly detected by neutrophils and/or macrophages/monocytes.

In an attempt to obtain further information about the possible role of C5a/C5aR1 signaling in the pathophysiology of COVID-19, we performed correlation analyses of C5a concentrations with different inflammatory markers/cells that we have previously shown to be enhanced in the BAL fluid of COVID-19 patients (29). Notably, C5a levels correlated with the number of hyperactivated/degranulating neutrophils (positive for CD66b and the tetraspanin CD63) (Supplementary Figure S4), and with the neutrophil attractant CXCL8 but not with any other inflammatory marker (Supplementary Figure S4). In agreement, hyperactivated neutrophils in the BAL fluid of COVID-19 patients were characterized by higher expression of CXCL8 and they seem to play a critical role in COVID-19 pneumonia (29, 34–36). Altogether, these data point towards a possible role for C5a in the hyperactivation of neutrophils in the lungs of COVID-19 patients.

C5a/C5aR1 signaling on myeloid cells has a detrimental role in a murine model of COVID-19

In order to better understand the importance and role of C5a/C5aR1 signaling on the pathophysiology of COVID-19, we moved to a well-established preclinical mouse model used to study this disease, the K18-hACE2 Tg mice (Tg) infected with SARS-CoV-2 (37, 38) (Figure 3A). As observed in BAL fluid from COVID-19 patients, the levels of C5a increased in the lungs of Tg mice infected with SARS-CoV-2 **(**Figure 3B**)**. We also detected increased levels of factor Bb and C3a in the lungs of SARS-CoV-2-infected Tg mice (Figure 3, C and D)**.**

We also noticed that clinical signals (clinical score, weight loss), lung dysfunction (reduction of oxygen saturation) and lung pathology (focal area of neutrophil infiltration into the alveolar space, type II alveolar epithelial cell proliferation, focal filling of the alveolar space with proteinaceous alveolar fluid and debris, and thickening of alveolar septae by inflammatory cells) worsened in the COVID-19 mouse model compared to non-infected mice (Supplementary Figure 5, A and B, and Supplementary Figure 6). These observations were associated with increased levels of pro-inflammatory cytokines/chemokines in the lungs of infected mice (Supplementary Figure 5C), as observed previously (37, 39, 40). The expression of C5aR1 in lung tissue of SARS-CoV-2 infected mice was also analyzed by immunofluorescence. $Tg^{Flox/Flox}$ mice (which contain an eGFP reporter for C5aR1 expression) were infected with SARS-CoV-2 and the lungs were collected at 5 days post infection (dpi). Similar to what we observed in the lung tissue of COVID-19 patients, immunofluorescence analyses of the lung tissue of

SARS-CoV-2-infected $Tg^{Flox/Flox}$ mice revealed that C5aR1 is mainly expressed in cells positive for NE (neutrophils, 41.2 ± 16.07 %) and Iba-1 (macrophages, 48.62 ± 15.07 %) (Figure 3, E and F). The C5aR1 seems to be expressed by 10.17 ± 6.08 % of unidentified cells (Figure 3F). These results indicate that during SARS-CoV-2 infection in mice, there may also be a local activation of C5a/C5aR1 signaling, especially in neutrophils and macrophages/monocytes.

Based on the fact that the pattern of expression of C5aR1 is mainly concentrated in myeloid cells (neutrophils and macrophages/monocytes) in the lung of COVID-19 patients and Tg mouse-infected by SARS-CoV-2, we developed a colony of Tg mice that lacks C5aR1 (Tg^{cKO} mice) signaling in these immune cells and they were infected with SARS-CoV-2 (Supplementary Figure 7A). Although we did not observe any difference in the weight loss or clinical score in Tg^{cKO}-infected mice compared to $Tg^{Flox/Flox}$ mice during the course of the disease (Supplementary Figure 7B), the histopathological analysis of the lung revealed a reduced level of tissue damage (Figure 3, G and I, and Supplementary Figure 6). In agreement with the histopathological data, the number of TUNEL positive cells in the lung tissue of Tg^{cKO} mice was also reduced when compared with the tissue of $Tg^{Flox/Flox}$ mice, indicating a reduction in cell death and consequently a reduction in the lung tissue damage (Figure 3, H and J). We performed ELISA assays to the cytokines that we noticed altered in the mouse model (Supplementary Figure 5C) and we observed that the reduction in COVID-19-related lung pathology in Tg^{cKO}-infected mice was also associated with a reduction in the levels of pro-inflammatory cytokines/chemokines, especially, CCL3, CCL4, CXCL1 and IL-6 (Figure 3K). No difference was observed in the viral load between $Tg^{Flox/Flox}$ and Tg^{cKO}-infected mice (Supplementary Figure 7C). These results indicated that C5aR1 signaling on myeloid cells is involved in the SARS-CoV-2-induced lung pathology but has no participation in the control of the virus infection.

A pharmacological C5aR1 antagonist ameliorates COVID-19 in the mouse model

Since C5a/C5aR1 signaling seems to be involved in the immunopathology of COVID-19, we sought to test the efficacy of DF2593A, an orally-acting and selective C5aR1 allosteric antagonist (41), on SARS-CoV-2-infected Tg mice to explore this candidate for the treatment of COVID-19. As a proof-of-concept experiment, we treated Tg mice with DF2593A 1 h before SARS-CoV-2 infection and once a day up to the day of sample collection (5 dpi) (Figure 4A). Notably, the treatment with DF2593A reduced the body

weight loss, improved the clinical score, and mitigated the reduction of oxygen saturation (Figure 4B) of the Tg-infected mice compared to vehicle-treated mice. This treatment also ameliorates lung pathology and reduces the number of dead cells (TUNEL+ cells) in the lung tissue of DF2593A-treated Tg-infected mice when compared to the vehicle-treated group (Figure 4, C - F, and Supplementary Figure 6), while it did not alter the viral load (Supplementary Figure 8A). Corroborating these results, *in vitro* data showed that DF2593A was also not effective to inhibit SARS-CoV-2 replication in Vero E6 cells (Supplementary Figure 8B). We performed ELISA assays to the cytokines that we noticed altered in the mouse model (Supplementary Figure 5C) and we observed that the reduction in lung pathology was also associated with a reduction in the levels of pro-inflammatory cytokines/chemokines, especially CCL3 and IL-6 in the lung tissue of mice treated with DF2593A (Figure 4G).

In a therapeutic perspective, we performed a post-infection treatment (starting 24 h after infection) of infected mice with DF2593A (Figure 5A). Although, we did not find significative difference in the clinical evolution of the disease and loss of body weight, the DF2593A post-infection mitigated the reduction of oxygen saturation (Figure 5B) and lung pathology (Figure 5, C and D, and Supplementary Figure S6) when compared to infected Tg mice treated with vehicle. These preclinical results indicate that pharmacological inhibition of C5aR1 could be a novel approach to ameliorate COVID-19.

C5a/C5aR1 signaling enhances NETs formation to aggravate COVID-19

C5a/C5aR1 signaling in myeloid cells (especially in neutrophils) is able to promote cell migration by triggering their arrest on the endothelium and/or chemotaxis (17, 42), suggesting it would be involved in the recruitment of these cells into the SARS-CoV-2 infected lungs. Thus, we further analyzed whether the lack of C5aR1 signaling in myeloid cells could impact the infiltration of these cells in the lung of SARS-CoV-2 infected Tg mice. Notably, FACS analyses revealed that the infiltration of total leukocytes (CD45+ cells), myeloid cells (CD45+CD11b+) as well as neutrophils (CD45+CD11b+Ly6G+ cells) and inflammatory monocytes (CD11b+CCR2+Ly6C+) was similar in the lung tissue of Tg^{cKO}-infected mice compared to $Tg^{Flox/Flox}$ mice (Supplementary Figure 9, A-D). Like what we have found in Tg^{cKO} mice, DF2593A treatment did not reduce the infiltration of total myeloid cells. Like what we have found in Tg^{cKO} mice, DF2593A treatment did not reduce the infiltration of total myeloid cells, neutrophils, or inflammatory monocytes (Supplementary Figure 9, E - G) in the lung tissue of Tg-

infected mice. On the other hand, the total leukocyte infiltration in the lung tissue of Tg-infected mice was reduced by DF2593A treatment compared to vehicle treatment (Supplementary Figure 9H). Together, these results indicated that C5aR1 signaling on myeloid cells is not crucial in the infiltration of these cells into the lung of SARS-CoV-2-infected Tg mice.

Our findings indicating that C5a/C5aR1 signaling in myeloid cells is involved in the lung immunopathology of COVID-19, but not in the infiltration of these cells into the lung, prompted us to hypothesize that this signaling would be involved in the local activation of these cells. Additionally, our finding that C5a levels in the BAL of COVID-19 patients correlate with degranulation of hyperactivated neutrophils and pro-inflammatory cytokines/chemokines (Supplementary Figure 4) also supports this hypothesis. Among the downstream mechanisms by which activated neutrophils might participate in the pathophysiology of COVID-19, the production of NETs is one of the most described (43, 44). In our lung tissue samples from COVID-19 patients, we also detected the presence of NETs (Supplementary Figure 10). Thus, we evaluated whether C5a/C5aR1 signaling would be involved in NETs formation in the lungs of SARS-CoV-2-infected Tg mice. Corroborating this hypothesis, we found that the levels of NETs in the lung tissue of Tg^{cKO}-infected mice were significantly reduced compared to the $Tg^{Flox/Flox}$-infected mice (Figure 6, A and B). Furthermore, we found that the lung tissue of Tg-infected mice treated with DF2593A has lower levels of NETs compared to the lung tissue from vehicle-treated mice (Figure 6, C and D).

Instillation of C5a in the mouse lungs has been shown to promote tissue inflammation and damage (45). To test that the deleterious effects of C5a described above are dependent on NETs *in vivo*, we treated C57BL6 mice twice with DNAse [NETs degrading agent (46)] or DF2593A following the intratracheal instillation of recombinant murine (rm) C5a (Figure 7A). Intratracheal instillation of rmC5a promoted lung pathology which was associated with the presence of NETs, and increased levels of CCL2 and CXCL1 (Figure 7, B - F). Both treatments (DNAse and DF2593A) reduced these alterations induced by mrC5a installation to the levels found in control animals (Figure 7, B - F). These results indicate that C5a-induced lung inflammation/pathology is dependent on NETs release through C5aR1 signaling.

The importance of NETs for the pro-inflammatory action of C5a/C5aR1 signaling in these models, described above, could be due to a direct or indirect effect on neutrophils. In this context, we evaluated the ability of C5a to induce NETs in an *in vitro* culture of human

blood-derived neutrophils. Notably, we found that the treatment of human neutrophils with recombinant human (rh) C5a promoted NETosis (Figure 8, A - C). Mechanistically, we found that rhC5a-induced NETosis was inhibited by the treatment of human neutrophils with DF2593A, CL-amidine (PAD4 inhibitor) and diphenyleneiodonium (DPI; Reactive oxygen species, ROS inhibitor) (Figure 8, A - C). In addition, neutrophils infected with SARS-CoV-2 produced higher levels of NETs in the presence of low concentration of rhC5a when compared to rhC5a treated neutrophils or infected neutrophils without addition of rhC5a (Figure 8, D - F). These results suggest that C5a via C5aR1 is able to directly promote NETosis through the stimulation of the canonical PAD4-ROS pathway. The data also indicate that in the SARS-CoV-2 infecting neutrophils, C5a/C5aR1 signaling might amplify the NETosis process. Altogether, these data indicate that the induction of NETs in the lung tissue of SARS-CoV-2-infected mice might be a crucial mechanism triggered by C5a/C5aR1 signaling that contributes to the pathophysiology of COVID-19.

Discussion

COVID-19 is caused by two main factors: the virus replication that *per se* causes cellular injury and the dysregulated inflammatory/immune response that amplifies the tissue/organ dysfunction, especially in the lung. Although there is a race to identify novel antiviral drugs capable to inhibit SARS-CoV-2 replication and then reduce COVID-19 severity, drugs that target the inflammatory/immune response, at least partially, have been shown effective in ameliorating COVID-19 (47–51). Thinking about drugs targeting the immune system to control COVID-19, it is desirable to identify immune cells/mediators and molecular mechanisms that are not involved in the control of virus infection (and possible secondary infection) but are critical for immunopathology. Among several inflammatory mediators that may possess these characteristics, we and others consider complement factor C5a, and its receptor C5aR1, among the most interesting candidates (11, 30). In agreement, targeting C5a/C5aR1 signaling ameliorates virus infection-induced lung diseases, including influenza A, MERS-CoV, and RSV (20–22). Herein, we confirmed this hypothesis showing that both genetic and pharmacological inhibition of C5a/C5aR1 signaling, especially in neutrophils, have a beneficial effect on a preclinical mouse model of COVID-19. In addition, we showed that this beneficial effect is likely due to a reduction in NETs formation.

The understanding of COVID-19 pathophysiology is one of the most important ways to identify critical targets for the development of novel drugs to treat this disease. In this context, our study provides evidence validating the hypothesis that C5a/C5aR1 signaling plays a detrimental role in COVID-19 and might be considered as an interesting candidate for novel treatments. Initially, we showed that C5aR1 signaling is selectively enhanced in the lung of COVID-19 patients compared to influenza virus patients, especially in neutrophils. These data are in agreement with previous reports showing higher levels of C5a in the plasma of COVID-19 patients, which correlate with disease severity (24, 52–54). Our data on the increase of factor Bb in the BAL fluid from COVID-19 patients are also consistent with the observation of systemic activation of the alternative complement pathway (55–57). In addition, our human data were validated in a well-accepted preclinical model of COVID-19, in which we also observed an increase in C5aR1 signaling activation in myeloid cells (especially neutrophils) in the lung after SARS-CoV-2 infection.

The increase in C5aR1 signaling in the lungs of patients and mice with COVID-19 led us to explore whether inhibition of this pathway would have a protective effect. Noteworthy, either the use of mice lacking C5aR1 signaling in myeloid cells (Tg^{cKO} mice) or the pharmacological inhibitor (the C5aR1 antagonist, DF2593A) provided beneficial effects. The dissociation between clinical parameters and lung pathology in Tg^{cKO}-infected mice, although discrepant, might be explained by the fact that while Tg mice infected with SARS-CoV-2 developed lung disease similar to COVID-19 patients, clinical signs that led to eventual morbidity/mortality are mainly due to the central nervous system (CNS) dysfunction (58, 59). In fact, high SARS-CoV-2 burden and encephalitis have been found also in the brains of these animals (58–60). This has been considered a limitation of this mouse model of COVID-19 (58). Alternatively, we cannot exclude that C5aR1 signaling in cell types, beyond neutrophils/macrophages, might also play a role in the pathophysiology of COVID-19 (61, 62). For instance, C5aR1 signaling in endothelial cells was found to be a prothrombogenic effector in COVID-19 patients (62). Thus, further studies will be necessary to address the role of C5a/C5aR1 signaling in cells other than myeloid cells in the pathophysiology of COVID-19. In addition, the higher efficacy of DF2593A on clinical parameters in Tg mice infected with SARS-CoV-2 compared to the phenotype observed in Tg^{cKO} mice is not immediately apparent, but it could be also explained by the fact that C5aR1 is expressed in cells other than myeloid cells, which are probably inhibited by the C5aR1 antagonist as well. Additionally, since we have

previously shown that DF2593A is able to cross the blood-brain barriers (41), it might also reduce brain inflammation which is, as we mentioned before, an important drawback of this COVID-19 mice model. Nevertheless, since central nervous system changes have been considered one of the important aspects of Long-COVID-19 (63) syndrome, the blockage of C5aR1 signaling, by DF2593A, could be an alternative to avoid the development of this condition. Supporting this hypothesis, in a mouse model of MERS-CoV infection, brain damage was reduced by an anti-C5aR1 murine antibody (64).

Regarding the mechanisms by which C5aR1 signaling is involved in the lung immunopathology during COVID-19, we ruled out the possibility that this pathway would be crucial in the recruitment of myeloid cells into the SARS-CoV-2-infected lungs. Indeed, no significant alteration in myeloid cells infiltration in the lungs of COVID-19 mice was observed either with genetic or pharmacological inhibition of C5aR1 signaling. This could be due the redundancy among the different inflammatory mediators such as neutrophil/monocytes-recruiting chemokines (e.g. CXCR2 ligands and CCL2), which are up-regulated in the lungs of SARS-CoV-2-infected mice (38, 64). On the other hand, the inhibition of C5aR1 by DF2593A in cells beyond myeloid cells might explain the reduction of total leukocyte infiltration caused by the pharmacological treatment. Indeed, C5aR1 signaling on non-myeloid cells might favor, directly or indirectly, the infiltration of non-myeloid leukocytes during COVID-19 in mice. Moreover, these non-myeloid cells (e.g. NK cells) can be harmful for the lung during COVID-19, as already demonstrated (65). This might also explain why DF2593A treated mice showed a better phenotype compared to the phenotype of Tg^{cKO}-infected mice.

Since C5a/C5aR1 signaling in myeloid cells is involved in the lung immunopathology of COVID-19, but not in the infiltration of these cells into the lung, we investigated its possible role in the local activation of these cells, focusing mainly on neutrophils. This hypothesis is based on previous evidence showing that: a) C5a/C5aR1 signaling directly triggers neutrophil activation (e.g. granule enzyme release and superoxide anion production/respiratory burst) in several pathological conditions (66–71); b) C5aR1 signaling induces neutrophils to degranulate (with increase in CD66 expression) in sepsis models (72); c) C5a levels in the soluble fraction of sputum correlated positively with markers associated with worse cystic fibrosis lung disease, including NE, MPO activity and DNA concentration (73). Additionally, our finding that C5a levels in the BAL of COVID-19 patients correlate with degranulated/hyperactivated neutrophils also supports this hypothesis. Among the downstream mechanisms by which activated neutrophils

might participate in the pathophysiology of COVID-19, the production of NETs is one of the most described (43, 44). For instance, we and others have previously shown that in the lung of COVID-19 patients, SARS-CoV-2 directly triggers NET-dependent lung immunopathology (46, 74–76). We also found that hyperactivated neutrophils in the BAL from COVID-19 patients are enriched for NET-related genes (34). Moreover, data from our lab also showed that Tg-infected mice treated with NETs-degrading DNase ameliorates lung pathology (46). Our present data showed that the inhibition of C5aR1 signaling in myeloid cells reduced the levels of NETs in the lung of SARS-CoV-2-infected mice. Corroborating, we also found that C5a alone, via C5aR1, is able to induce lung inflammation/pathology in NETs-dependent manner *in vivo.* These results raised the question whether the C5a/C5aR1 signaling is driving NETs formation in a direct or indirect manner. In this context, we found that a low dose of C5a was able to promote NETs formation by naive human neutrophils *in vitro*, in a C5aR1 dependent manner. Mechanistically, C5a-triggered NETs in human neutrophils seem to be dependent on the PAD4/ROS canonical pathway. These findings are in agreement with evidence that plasma from COVID-19 patients triggers NETs formation by human naive neutrophils, and this was reduced by inhibition of C5aR1 signaling (77). Although these data strongly indicate that C5a/C5aR1 signaling directly causes NETs formation and this mechanism is important for the inflammatory activity of this signaling, we cannot exclude an indirect effect of C5a on NETs formation. In addition, we have also shown that *in vitro* infection of naive human neutrophils with SARS-CoV-2 promoted NETs formation and this effect was dependent on the replication process, although the replication was not completed (abortive replication) (46). Herein, we also found that C5a enhances NETs formation by human neutrophils infected with SARS-CoV-2. These results suggest that in the lung of COVID-19 patients (and SARS-CoV-2 infected mice) the presence of infected-neutrophils and higher levels of C5a might amplify the NETosis process. Although, our data indicate the importance of C5aR1 signaling in neutrophils triggering NETs that in turn contributes for the pathophysiology of COVID-19, it is noteworthy that in Tg^{cKO} mice, C5aR1 signaling is also interrupted in macrophages/monocytes (78). Therefore, we cannot exclude that part of the protective phenotype observed in the Tg^{cKO}-infected mice would be due to inhibition of C5aR1 signaling in those cells that indirectly might also affect NETs production.

The fact that targeting C5aR1 signaling in SARS-CoV-2-infected mice, besides to inhibit NETs formation in the lung, it also reduced the increase in the levels of pro-inflammatory

cytokines/chemokines raised the question whether NETs intermediate this process. Notably, our current data showing that lung inflammation promoted by C5a instillation (including increased chemokines levels) was prevented by NETs degradation favor this possibility. However, since we do not have the entire time course of C5a-induced lung inflammation, we could not exclude the possibility that C5a might induce an initial release of cytokines that in turn promote NETs. Subsequently, NETs could amplify the inflammatory process by promoting tissue damage and additional cytokines/chemokines production. In fact, there is evidence that NETs may amplify inflammation through tissue damage (78–81), including triggering direct cytokines/chemokines production (79, 80). Based on our data and previous data from the literature, our current hypothesis is that SARS-CoV-2 infection may trigger initial production of some cytokines and chemokines that promote neutrophil infiltration. At the local of infection (lungs), neutrophils are activated by C5a to produce NETs (which may also synergize with virus infection), which promote tissue damage and could also amplify the inflammatory process.

Our data further reinforce the possibility to use inhibitors of C5a/C5aR1 signaling for the treatment of COVID-19. In fact, clinical results show that inhibition of C5a reduced COVID-19 hyper-inflammation and improved lung function (25–27). Notably, a Phase 3 clinical study has been shown that treatment of severe COVID-19 patients with Vilobelimab, an anti-C5a monoclonal antibody, significantly reduced mortality (28). The hypothesis that the blockage of C5aR1 signaling would be beneficial to COVID-19 may open another important question related to secondary infections that are extremely common in COVID-19 patients and are a critical threat in the current treatments targeting the immune response (81–85). Although, inhibition of C5 by neutralizing antibodies has been associated with increased risk of bacterial infection due to the inhibition of the formation of the membrane attack complex, the selective targeting of C5a/C5aR1 signaling may avoid harmful anaphylatoxin-induced effects (86, 87). In fact, inhibition of C5aR1 signaling reduced the consequences of exacerbated bacterial infection such as observed in sepsis (88–91). These studies gave support for the hypothesis that C5a/C5aR1 signaling is more important for immunopathology (tolerance) than for immune defense against infections (resistance).

Overall, our study provides direct evidence of the detrimental role C5a/C5aR1 signaling for the lung immunopathology in COVID-19. It also provides the molecular mechanism by which C5aR1 signaling, especially in neutrophils via NETs-dependent lung pathology, mediates COVID-19 pathophysiology. In conclusion, our study confirms that inhibition

of C5aR1 signaling, for example by orally active allosteric inhibitors, could be alternative therapeutics against this disease.

Material and Methods

COVID-19 mouse model

K18-hACE2 transgenic (Tg) mice (B6.Cg-Tg(K18-ACE2)2Prlmn/J, cat. 034860) and *Lyz2*$^{Cre/Cre}$ (B6.129P2-Lyz2tm1(cre)Ifo/J, cat. 004781) mice were purchased from Jackson Laboratory. *C5ar1*$^{Flox/Flox}$ mice, which also express eGFP under the C5aR1 promoter, were kindly donated by Prof. Jörg Köhl (92). To generate Tg^{cKO} and $Tg^{Flox/Flox}$ (littermate controls), Tg mice were bred with *Lyz2*$^{Cre/0}$*C5ar1*$^{Flox/Flox}$ mice. Local colonies of transgenic mice were established and maintained at the Animal Care Facility of Ribeirão Preto Medical School, University of São Paulo. Food and water were available *ad libitum* and mice kept in a controlled light-dark cycle. For COVID-19 induction, the animals received intranasal inoculation of SARS-CoV-2 (2 x 10^4 PFU) which presents disease signs and lung pathology consistent with human disease. The manipulation of these animals was performed in a Biosafety Level 3 (BSL3) facility.

Human and mouse C5a, factor Bb and C3a levels quantification

The C5a, factor Bb and C3a levels were determined in the BAL fluid and plasma from sixteen critically ill adult patients with COVID-19 (<20 days in intensive care unit - ICU) and sixteen patients with influenza, as a non–COVID-19 viral pneumonia cohort. Both patient cohorts have been described previously (29). C5a factor Bb, and C3a ELISA assays were performed using, respectively, the kit from R&D Systems (cat. DY2037), from Quidel (cat. #A027), and from ThermoFisher Scientific (cat. #BMS2089). All assays were performed according to the manufacturer's instructions.

For mice, lung homogenate was obtained and the supernatant was collected. ELISA assays were performed to detect the concentration of C5a, factor Bb, and C3a using a kit from R&D Systems (cat. DY2150, cat. NBP2-75243, and cat. CTK-148, respectively), according to the manufacturer's instructions.

Virus stock production

SARS-CoV-2 (Brazil/SPBR-02/2020 strain) was kindly provided by Prof. Edison Luiz Durigon (ICB-USP, Sao Paulo). The virus was propagated and titrated in Vero E6 cells in a biosafety level 3 laboratory (BSL3) at the Center for Virus Research, Ribeirao Preto

Medical School (Ribeirao Preto, Brazil). Cells were cultured in DMEM medium (Corning; cat. 15-013-CVR) supplemented with 10 % fetal bovine serum (FBS; GE Life Sciences; cat. SV30160.03) and antibiotic/antimycotic (Penicillin 10,000 U/ml; Streptomycin 10,000 µg/ml; Sigma-Aldrich; cat. P4333). The viral inoculum was added to Vero cells in DMEM (FBS 2%) incubated at 37 °C with 5 % CO_2 for 48 h. The cytopathogenic effect was observed under a microscope. A cell monolayer was collected, and the supernatant was stored at -70 ºC. Virus titration was performed by calculating the plaque-forming units (PFU).

Drugs and pharmacological treatment *in vivo*

For *in vivo* experiments, we used DF2593A (3 mg/kg p.o), a selective C5aR1 antagonist (41). For the COVID-19 mouse model, the drug was administered 1 h before or 24 h after SARS-CoV-2 inoculation and daily post-infection. We assessed the daily: clinical scores (Supplementary Table 1) and body weight of each animal. We also evaluated the oxygen saturation pior to the infection and daily post-infection using a mouse pulse oximeter (MouseOx® Plus, Starr Life Sciences, USA). At 5 days post-infection, lungs from mock and SARS-CoV-2-infected mice were collected. Lung lobules were collected, harvested, and homogenized in PBS with steel glass beads. The homogenate was added to TRIzol reagent (1:1; Invitrogen; cat. 15596026), for posterior viral titration via RT-qPCR, or to lysis buffer (1:1), for the ELISA assay, and stored at -70 °C. In another cohort experiment, the left lung was collected in paraformaldehyde (PFA 4 %; Millipore; cat. 818715) for posterior histological assessment.

***In vitro* SARS-CoV-2 infection**

Vero E6 cells ($1x10^5$) were pretreated with DF2593A at 0.01; 0.1; 1.0; 10.0 µM for 1 h prior to SARS-CoV-2 infection at 37 ºC. Cells were infected at a multiplicity of infection (MOI) of 1.0 with infectious clone SARS-CoV-2 or mock with infection media to evaluate viral load by RT-PCR, 24 h post-infection. The treatment was performed in technical quadruplicate.

SARS-CoV-2 viral load

SARS-CoV-2 detection was performed with primer-probe sets for 2019-nCoV_N1 and N2 (Integrated DNA Technologies; cat. 10006713), according to the US Centers for Disease Control (CDC) protocol by RT-PCR, using total nucleic acids extracted with

Trizol reagent from cell pellet or lung tissue to determine the genome viral load. All RT-PCR assays were done using the Viia 7 Real-time PCR System (Applied Biosystems). A standard curve was generated in order to obtain the exact number of copies in the tested sample. The standard curve was performed using an amplicon containing 944 bp cloned in a plasmid (PTZ57R/T CloneJetTM Cloning Kit Thermo Fisher®), starting in the nucleotide 14 of the gene N. To quantify the number of copies, a serial dilution of the plasmid in the proportion of 1:10 was performed. Commercial primers and probes for the N1 gene and RNAse P (endogenous control) were used for the quantification (2019-nCov CDC EUA Kit, Integrated DNA Technologies), following the CDC's instructions.

***In vivo* challenge with rmC5a:** C57BL6 male mice (8 weeks-old) were treated with DNAse (Pulmozyme®, 10 mg/kg, s.c.) twice before the challenge with rmC5a (400 nM) by intratracheal instillation (45) (treatment administered 24 h and 1 h before rmC5a). Eight hours after the challenge, lungs were collected and fixed in PFA 4 % for subsequent histological analysis. Five micrometer slices were, then, submitted to hematoxylin and eosin staining, and images were taken under a brightfield microscope. In another set of animals, we performed the same experiment and collected lungs for ELISA assay. The sandwich ELISA method was performed to detect the concentration of cytokines and chemokines using kits from R&D Systems (DuoSet), according to the manufacturer's instructions. The following targets were evaluated: CCL2, CCL3, CCL4, CXCL1, and IL-6.

Re-analysis of scRNA-seq data sets

We re-analyzed single-cell transcriptomic data from BAL fluid cells from patients with severe COVID-19 and their respective control groups (31, 33). The dataset was downloaded and the RDS file was imported into R environment version v4.04 and Seurat v4.1.1 (98) by filtering genes expressed in at least 3 cells and more than 200 unique molecular identifiers (UMI) counts per cell. For the pre-processing step, outlier cells were filtered out based on three metrics (library size < 60000, number of expressed genes between 200 and 7500, and mitochondrial percentage expression < 20). The top 3,000 variable genes were then identified using the 'vst' method using the FindVariableFeatures function. Percent of mitochondrial genes was regressed out in the scaling step, and Principal Component Analysis (PCA) was performed using the top 3,000 variable genes with 40 dimensions. Additionally, a clustering analysis was performed on the first 7

principal components using a resolution of 2 followed by t-Distributed Stochastic Neighbor Embedding (tSNE), a dimensionality reduction technique for data visualization. Then, differential gene expression analysis was performed using FindAllMarkers function with default parameters to obtain a list of significant gene markers for each cluster of cells. To account for the frequency of cells expressing C5AR1, we filtered cells with raw counts of C5AR1>0. The dataset generated by authors is publicly available at: 1 the EGA European Genome-Phenome Archive database (EGAS00001004717 accessible at: https://ega-archive.org/studies/EGAS00001004717) or at http://covid19.lambrechtslab.org/.; 2) at https://covid19-balf.cells.ucsc.edu/.

Human lung samples from autopsies

We performed adapted minimally invasive autopsies from 4 COVID-19 fatal cases (93). (Supplementary Table 2). Briefly, a mini-thoracotomy (3 cm) was done under the main area of lung injury identified by prior ultrasound. The lung parenchyma was clamped by Collins Forceps, cut, and fixed in 10% buffered formalin (Sigma-Aldrich; cat. 252549).

H&E staining and lung pathology

Lung slices (5 μm) were fixed with PFA 4%, paraffin-embedding, and submitted to Hematoxylin and Eosin (H&E) staining. The morphological analysis was based on the Standards for Quantitative Assessment of Lung Structure published by ATS/ERS (100). Briefly, a systematic uniform random sampling of the lungs was performed. Considering uniform lung inflation and fixation in 10 % buffered formalin, 10 high-power field photographs were taken of the H&E slides of each case, followed by selection of the septal component and determination of its area versus total area using the Image Pro Plus software. The ratio between total septal area and the total lung area was expressed as area fraction (%). The mean area fraction values between the 10 high-power field photographs from each animal were used for statistical comparison between groups and for graphical representation. Additional histological evaluation was performed by an expert pathologist.

Immunostaining and confocal microscopy

Lung samples from COVID-19 autopsies or $Tg^{Flox/Flox}$-infected mice were fixed with PFA 4 %. After dehydration and paraffin embedding, 5-μm sections were prepared. The slides were deparaffinized and rehydrated by immersing the through Xylene (Labsynth; cat.

00X1001.06.BJ) and 100 % Ethanol (Labsynth; cat. 00A1084.07.BJ) for 15 min with each solution. Antigen retrieval was performed with 1.0 mM Ethylene Diamine Tetra Acetic acid (EDTA; Labsynth; cat. 00E1005.06.AG) 10 mM Trizma-base (Sigma-Aldrich; cat. T1503), pH 9.0 at 95 °C for 30 min. Afterward, endogenous peroxidase activity was quenched by incubation of the slides in 5 % H_2O_2 in methanol (Millipore; cat. 106009) at RT for 20 min. After blocking with IHC Select Blocking Reagent (Millipore, cat. 20773-M) at RT for 2 h, primary antibodies were incubated overnight at 4 °C: mouse monoclonal anti-C5aR1 (clone: S5/1; Millipore; cat. MABF1980; 1:50), rabbit polyclonal anti-IBA1 (FUJIFILM Wako Pure Chemical Corporation; cat. 016-20001; 1:200), rabbit polyclonal anti-NE (Abcam; cat. ab68672; 1:100), goat polyclonal anti-MPO (R&D Systems, cat. AF3667, 1:100) and rabbit polyclonal, anti-histone H3 (H3Cit; Abcam; cat. ab5103; 1:100). The slides were washed with TBS-T (Tris-Buffered Saline with Tween 20) and incubated with secondary antibodies alpaca anti-mouse IgG Alexa Fluor 594 (Jackson ImmunoResearch; cat. 615-585-214; 1:1,000), donkey anti-goat IgG Alexa Fluor 488 (Abcam, cat. ab150129), alpaca anti-rabbit IgG AlexaFluor 488 (Jackson ImmunoReseacher; Cat. 611-545-215; 1:1,000) and alpaca anti-rabbit IgG AlexaFluor 594 (Jackson ImmunoReseacher; Cat. 611-585-215; 1:1,000). Autofluorescence was quenched using the TrueVIEW Autofluorescence Quenching Kit (Vector Laboratories, cat. SP-8400-15). The percentage of cells expressing C5aR1 was determined by colocalization between Iba1 (macrophage) or NE (neutrophil) with C5aR1 expression. Four randomized fields from four COVID-19 fatal cases or $Tg^{Flox/Flox}$-infected mice were analyzed.

For NETs detection *in vitro*, neutrophils were plated in 24-well plates containing glass coverslips covered with 0.01% poly-L-lysine solution (Sigma-Aldrich; cat. P8920), fixed with PFA 4 % at RT for 10 min, 2 % bovine serum albumin (BSA; Sigma-Aldrich; cat. A7906) and 22.52 mg/ml glycine (Sigma-Aldrich; cat. G8898) in PBST (Phosphate Buffer Saline + 0.1% Tween 20) at RT for 2 h. The coverslips were stained with the following antibodies: rabbit polyclonal anti-Neutrophil Elastase (anti-NE; Abcam; cat. ab68672; 1:500), mouse monoclonal anti-MPO (2c7; Abcam; cat. ab25989, 1:800). After this, samples were washed in PBS and incubated with secondary antibodies: alpaca anti-mouse IgG AlexaFluor 488 (Jackson ImmunoReseacher; Cat. 615-545-214; 1:1,000) and alpaca anti-rabbit IgG AlexaFluor 594 (Jackson ImmunoReseacher; Cat. 611-585-215; 1:1,000). Slides were then mounted using ProLong™ Diamond Antifade Mountant with DAPI (Molecular Probes™, Thermo Fischer Scientific, Cat.P36962). Images were

acquired by Axio Observer combined with LSM 780 confocal microscope (Carl Zeiss) at 630X magnification at the same setup of zoomed, laser rate and scanned with 4 fields/image (tile scan function). NETs were quantified by the ratio between the total number of cells per field versus the number of NETosis (cells with loss of nucleus segmentation, cells in the process of releasing chromatin in networks) (NETosis = Cells / Cells in NETosis x 100). Images acquired and analyzed using Fiji by Image J.

Apoptosis TUNEL assay

Frozen lung tissue slices were used for the detection of apoptotic cells *in situ* with Click-iT Plus TUNEL Assay Alexa Fluor 488, according to the manufacturer's instructions (Thermo Fisher Scientific; cat. C10617). The slides were counterstained with Vectashield Antifade Mounting Medium with DAPI. Images were acquired by microscope Leica DMI6000B (Leica microsystems) at 200X magnification at the same laser rate. Ten fields (322.8 μm2 each) of the left lung were analyzed using Fiji by Image J, which represents 75 % of the total area of the left lung. The apoptosis quantification was performed as the percentage of TUNEL positive cells from DAPI staining.

Production of NETs by isolated human neutrophils

Blood samples were collected from healthy controls by venipuncture for in vitro experiments. Neutrophils were isolated and purified by Percoll density gradient (72 %, 63 %, 54 %, and 45 %) (GE Healthcare; Cat. 17-5445-01). Isolated neutrophils were resuspended in RPMI 1640 (Corning; cat. 15 040-CVR). Neutrophil purity was >95 % as determined by Rosenfeld's Color Cytospin (Laborclin; cat. 620529). A total of 1×10^6 isolated neutrophils were attached to coverslips coated with poly-L-lysine solution 0.1 % (Sigma-Aldrich; cat. P8920) incubated for 4 h at 37 °C for NET immunostaining.

Protocol 1: Isolated human neutrophils were incubated with the PAD4 inhibitor CL-amidine (200 μM), with the ROS production inhibitor DPI (10 μM/mL), or with the C5aR1 antagonist DF2593A (1 μM) for 1 h and, subsequently, challenged with rhC5a (3 nM; R&D; cat. 2037-C5-025/CF). The concentration of rhC5a was based on a concentration-response curve. Four hours after the challenge, supernatant was collected and stored at -80 °C. Cells were collected on a coverslip and, further, submitted to immunofluorescence for the visualization of NETs.

Protocol 2: Neutrophils were incubated with Mock, rhC5a (3 nM) or infected with SARS-CoV-2 (MOI = 1.0). One group of cells was incubated with SARS-CoV-2 and treated

with rhC5a (3 nM). Four hours after the challenge, supernatant was collected and stored at -80 °C. Cells were collected on a coverslip and, further, submitted to immunofluorescence for the visualization of NETs.

NETs quantification in the lung tissue

The 96 well black plates were coated with anti-MPO antibody (Thermo Fisher Scientific; cat. PA5-16672) (1:1000) overnight at 4 ºC. Subsequently, the plate was washed with PBS + 0.1 % Tween 20 and blocked with 2 % BSA for 2 h at RT. The lung tissue homogenates were obtained and centrifuged at 10,000 g at 4 °C for 10 min. Then, the supernatant was collected and incubated overnight at 4 ºC. On the third day, MPO-bound DNA (NETs) was quantified using the Quant-iT PicoGreen kit (Invitrogen; cat. P11496) as previously described (45).

Flow cytometry analysis

Lung tissue was harvested and digested with type 2 collagenase (1 mg/ml, Worthington; cat. LS004177) for 45 min at 37 ºC to acquire cell suspensions. Total lung cells (1 x 10^6) were then stained with Fixable Viability Dye eFluor 780 (Invitrogen; cat. 65–0865-14; 1:1000) and monoclonal fluorochrome-stained antibodies specific for CD45 (BD Pharmingen; clone 30F-11; cat. 553080; 1:200), CD11b (Biolegend; clone M1/70; cat. 101212; 1:200), Ly6G (Biolegend; clone 1A8; cat. 127606; 1:200), CCR2 (Biolegend; clone: SA203G11; cat. 150605; 1:200), Ly6C (eBioscience; clone: HK1.4; cat. 45-5932-82; 1:200), for 30 min at 4 °C. Data was acquired on FACSVerse flow cytometer (BD Biosciences) and analysis was performed using FlowJo (TreeStar) software. Gating strategies for flow cytometry analysis are schematically represented in (Supplementary Figure 11).

Cytokine and chemokine quantification

Lung homogenate was added to the RIPA buffer in the proportion of 1:1, and then centrifuged at 10,000 g at 4 °C for 10 min. The supernatant was collected and stored at -70 °C until use. The sandwich ELISA method was performed to detect the concentration of cytokines and chemokines using kits from R&D Systems (DuoSet), according to the manufacturer's instructions. The following targets were evaluated: CCL2, CCL3, CCL4, CXCL1, CXCL2, IFN-β, IL-6, IL-10, and TNF.

Statistics

Statistical significance was determined by either one or two-tailed unpaired and paired Student t-test, one-way or two-way ANOVA followed by Bonferroni's post hoc test. Spearman correlation analysis was performed by calculating a repeated measures correlation coefficient (r-value) and was plotted utilizing a simple linear regression line. $P<0.05$ was considered statistically significant. Statistical analyses and graph plots were performed and built with GraphPad Prism 9.3.1 software.

Study approval

Experimental procedures were performed in accordance with the guide for the use of laboratory animals of the University of Sao Paulo and approved by the ethics committee under protocol numbers 021/2021.

The use of human samples was approved by the Ethics Committee of the University Hospitals Leuven under the protocol S63881. Written informed consent was obtained from all study participants or their legal representatives according to the ethical guidelines of the Declaration of Helsinki. Minimally invasive autopsies were approved by the Ribeirão Preto Medical School Ethical Committee (protocol no. 4.089.567).

Data availability

The data supporting the findings are available within the paper and its supplementary information files or otherwise stated.

Acknowledgments

The authors gratefully acknowledge the technical assistance of Ieda R. Schivo, Ana Katia dos Santos, Jenna M. Turner, Sergio R. Rosa, Diva A. Sousa, Eleni Tamburus, Marcella Daruge Grando, Soraya Jabur, Felipe Souza, and Andreia Nogueira.

Funding

The research leading to these results received funding from a research grant from Dompé Farmaceutici s.p.a (USP/Dompé Farmaceutici s.p.a agreement), KU Leuven (C1 grant C16/17/010) and the São Paulo Research Foundation (FAPESP) under grant agreements n. 2020/04860-8 (COVID-19 project) and 2013/08216-2 (Center for Research in Inflammatory Disease) and a joint grant between FAPESP and Research Foundation Flanders (FWO Vlaanderen) (grant G0F7519N - 18/10990-1). SC is

supported by a PhD fellowship from FWO-Vlaanderen.

Competing interests

L.B. A.A., and M.A. are employees of Dompe Farmaceutici s.p.a... T.M.C. received a scientific grant from Dompé Farmaceutici s.p.a. Other authors declare no competing interests.

Author contributions

T.M.C, B.M.S, F.P.V and G.F.G designed, performed experimental work, analyzed data, and prepared the manuscript. B.M.S, F.P.V, G.F.G, D.B.C, D.C.N and G.V.L.S performed experimental work related to FACS and analyzed data. B.M.S, F.P.V and G.F.G performed experiments related to infection and harvested tissue. S.C and F.B performed experiments with BAL samples, including ELISA assays. B.M.S and G.F.G performed ELISA assay in mouse samples. G.V.L.S, I.M.S.C, PVM, H.I.N, and D.L. performed the single-cell transcriptome analysis. A.H.S, J.C.S and C.M.S performed neutrophil isolation and NETs quantification. F.P.V and J.C.S performed immunostaining and confocal analysis. F.P.V performed TUNEL assay. S.S.B and A.T.F contributed to lung autopsy analysis and histopathological analyses. B.M.S, S.D, I.M.P and R.M performed SARS-CoV-2 viral load and viral stock. B.M.S performed *in vitro* infections. A.U.Q and J.K performed Tg^{cKO} mice generation. P.L-J, R.D.O, P.P, E.W, L.V, S.F and J.W contributed to the collection of clinical specimens and demographic and clinical characteristics analysis from COVID-19 and influenzas patients. T.R, A.S, D.S.Z, L.O.L, J.C.A-F, E.A, L.D.C, L.B, A.A., F.Q.C performed experiments and important scientific comments. M.A, L.B, E.A, F.Q.C provided critical materials and comments. T.M.C designed, directed, and supervised the study, interpreted data, and wrote the manuscript. All authors reviewed the manuscript and provided final approval for submission.

Supplementary material

Supplementary material is available online.

Reference

1. Hu B, Guo H, Zhou P, Shi ZL. Characteristics of SARS-CoV-2 and COVID-19. *Nat. Rev. Microbiol.* 2021;19(3):141–154.

2. Berlin DA, Gulick RM, Martinez FJ. Severe Covid-19. *N. Engl. J. Med.*

788 2020;383(25):2451–2460.
789 3. Valle DM Del et al. An inflammatory cytokine signature predicts COVID-19 severity
790 and survival. *Nat. Med.* 2020;26(10):1636–1643.
791 4. Paludan SR, Mogensen TH. Innate immunological pathways in COVID-19
792 pathogenesis. *Sci. Immunol.* 2022;7(67).
793 5. van de Veerdonk FL et al. A guide to immunotherapy for COVID-19. *Nat. Med.*
794 2022;28(1):39–50.
795 6. Chen C-C, Yang Y-P, Tsai H-L, Tung T-H. Effects of Tocilizumab on Adults With
796 COVID-19 Pneumonia: A Meta-Analysis. *Front. Med.* 2022;9.
797 7. Karakike E et al. ESCAPE: An Open-Label Trial of Personalized Immunotherapy in
798 Critically lll COVID-19 Patients. *J. Innate Immun.* 2021;71.
799 8. Durán-Méndez A et al. Tocilizumab reduces COVID-19 mortality and pathology in a
800 dose and timing-dependent fashion: a multi-centric study. *Sci. Rep.* 2021;11(1).
801 9. Shankar-Hari M et al. Association Between Administration of IL-6 Antagonists and
802 Mortality Among Patients Hospitalized for COVID-19: A Meta-analysis. *JAMA*
803 2021;326(6):499–518.
804 10. Horby P et al. Dexamethasone in Hospitalized Patients with Covid-19. *N. Engl. J.*
805 *Med.* 2021;384(8):693–704.
806 11. Afzali B, Noris M, Lambrecht BN, Kemper C. The state of complement in COVID-
807 19. *Nat. Rev. Immunol.* 2022;22(2):77–84.
808 12. Lim EHT et al. Complement activation in COVID-19 and targeted therapeutic
809 options: A scoping review. *Blood Rev.* 2022;57.
810 13. Ostrycharz E, Hukowska-Szematowicz B. New Insights into the Role of the
811 Complement System in Human Viral Diseases. *Biomolecules* 2022;12(2):226.
812 14. Gerard C, Gerard NP. C5A anaphylatoxin and its seven transmembrane-segment
813 receptor. *Annu. Rev. Immunol.* 1994;12:775–808.
814 15. Soruri A, Kim S, Kiafard Z, Zwirner J. Characterization of C5aR expression on
815 murine myeloid and lymphoid cells by the use of a novel monoclonal antibody.
816 *Immunol. Lett.* 2003;88(1):47–52.
817 16. Vandendriessche S, Cambier S, Proost P, Marques PE. Complement Receptors and
818 Their Role in Leukocyte Recruitment and Phagocytosis. *Front. cell Dev. Biol.* 2021;9.
819 17. Sadik CD, Miyabe Y, Sezin T, Luster AD. The critical role of C5a as an initiator of
820 neutrophil-mediated autoimmune inflammation of the joint and skin. *Semin. Immunol.*
821 2018;37:21–29.

18. Mulligan MS et al. Requirement and role of C5a in acute lung inflammatory injury in rats. *J. Clin. Invest.* 1996;98(2):503–512.
19. Song N et al. C5a receptor1 inhibition alleviates influenza virus-induced acute lung injury. *Int. Immunopharmacol.* 2018;59:12–20.
20. Hu X et al. Respiratory Syncytial Virus Exacerbates OVA-mediated asthma in mice through C5a-C5aR regulating CD4 + T cells Immune Responses. *Sci. Rep.* 2017;7(1).
21. Garcia CC et al. Complement C5 activation during influenza A infection in mice contributes to neutrophil recruitment and lung injury. *PLoS One* 2013;8(5).
22. Jiang Y et al. Blockade of the C5a-C5aR axis alleviates lung damage in hDPP4-transgenic mice infected with MERS-CoV. *Emerg. Microbes Infect.* 2018;7(1).
23. Carvelli J et al. Association of COVID-19 inflammation with activation of the C5a-C5aR1 axis. *Nature* 2020;588(7836):146–150.
24. Cugno M et al. Complement activation in patients with COVID-19: A novel therapeutic target. *J. Allergy Clin. Immunol.* 2020;146(1):215–217.
25. De Leeuw E et al. Efficacy and safety of the investigational complement C5 inhibitor zilucoplan in patients hospitalized with COVID-19: an open-label randomized controlled trial. *Respir. Res.* 2022;23(1).
26. Memon AA et al. A Randomized Control Trial of Ravulizumab for Treatment of Patients With COVID-19 Infection and Kidney Injury. *Kidney Int. Reports* 2022;7(12):2714–2717.
27. Vlaar APJ et al. The anti-C5a antibody vilobelimab efficiently inhibits C5a in patients with severe COVID-19. *Clin. Transl. Sci.* 2022;15(4):854–858.
28. Vlaar APJ et al. Anti-C5a antibody (vilobelimab) therapy for critically ill, invasively mechanically ventilated patients with COVID-19 (PANAMO): a multicentre, double-blind, randomised, placebo-controlled, phase 3 trial. *Lancet Respir. Med.* 2022;10(12):1137–1146.
29. Cambier S et al. Atypical response to bacterial coinfection and persistent neutrophilic bronchoalveolar inflammation distinguish critical COVID-19 from influenza. *JCI insight* 2022;7(1).
30. Woodruff TM, Shukla AK. The Complement C5a-C5aR1 GPCR Axis in COVID-19 Therapeutics. *Trends Immunol.* 2020;41(11):965–967.
31. Wauters E et al. Discriminating mild from critical COVID-19 by innate and adaptive immune single-cell profiling of bronchoalveolar lavages. *Cell Res.* 2021;31(3):272–290.

856 32. Chaudhary N, Jayaraman A, Reinhardt C, Campbell JD, Bosmann M. A single-cell
857 lung atlas of complement genes identifies the mesothelium and epithelium as prominent
858 sources of extrahepatic complement proteins. *Mucosal Immunol.* 2022;15(5):927–939.
859 33. Liao M et al. Single-cell landscape of bronchoalveolar immune cells in patients with
860 COVID-19. *Nat. Med.* 2020;26(6):842–844.
861 34. Vanderbeke L et al. Monocyte-driven atypical cytokine storm and aberrant
862 neutrophil activation as key mediators of COVID-19 disease severity. *Nat. Commun.*
863 2021;12(1).
864 35. Cui SN, Tan HY, Fan GC. Immunopathological Roles of Neutrophils in Virus
865 Infection and COVID-19. *Shock* 2021;56(3):345–351.
866 36. Diamond B. The renin-angiotensin system: An integrated view of lung disease and
867 coagulopathy in COVID-19 and therapeutic implications. *J. Exp. Med.* 2020;217(8).
868 37. Winkler ES et al. SARS-CoV-2 infection of human ACE2-transgenic mice causes
869 severe lung inflammation and impaired function. *Nat. Immunol.* 2020;21(11):1327–
870 1335.
871 38. Zheng J et al. COVID-19 treatments and pathogenesis including anosmia in K18-
872 hACE2 mice. *Nature* 2021;589(7843):603–607.
873 39. Puhl AC et al. Pyronaridine Protects against SARS-CoV-2 Infection in Mouse. *ACS*
874 *Infect. Dis.* 2022;8(6):1147–1160.
875 40. Puhl AC et al. Vandetanib Blocks the Cytokine Storm in SARS-CoV-2-Infected
876 Mice [Internet]. *ACS Omega* 2022;7(36):31935–31944.
877 41. Moriconi A et al. Targeting the minor pocket of C5aR for the rational design of an
878 oral allosteric inhibitor for inflammatory and neuropathic pain relief. *Proc. Natl. Acad.*
879 *Sci. U. S. A.* 2014;111(47):16937–16942.
880 42. Heit B, Tavener S, Raharjo E, Kubes P. An intracellular signaling hierarchy
881 determines direction of migration in opposing chemotactic gradients. *J. Cell Biol.*
882 2002;159(1):91–102.
883 43. Veras FP et al. SARS-CoV-2-triggered neutrophil extracellular traps mediate
884 COVID-19 pathology. *J. Exp. Med.* 2020;217(12). doi:10.1084/jem.20201129
885 44. Ackermann M et al. Patients with COVID-19: in the dark-NETs of neutrophils. *Cell*
886 *Death Differ.* 2021;28(11):3125–3139.
887 45. Russkamp NF et al. Experimental design of complement component 5a-induced
888 acute lung injury (C5a-ALI): A role of CC-chemokine receptor type 5 during immune
889 activation by anaphylatoxin. *FASEB J.* 2015;29(9):3762–3772.

890 46. Veras FP et al. Targeting neutrophils extracellular traps (NETs) reduces multiple
891 organ injury in a COVID-19 mouse model [Internet]. *Respir. Res.* 2023;24(1).
892 47. Tomazini BM et al. Effect of Dexamethasone on Days Alive and Ventilator-Free in
893 Patients With Moderate or Severe Acute Respiratory Distress Syndrome and COVID-
894 19: The CoDEX Randomized Clinical Trial. *JAMA* 2020;324(13):1307–1316.
895 48. Salama C et al. Tocilizumab in Patients Hospitalized with Covid-19 Pneumonia. *N.*
896 *Engl. J. Med.* 2021;384(1):20–30.
897 49. Kyriazopoulou E et al. Early treatment of COVID-19 with anakinra guided by
898 soluble urokinase plasminogen receptor plasma levels: a double-blind, randomized
899 controlled phase 3 trial. *Nat. Med.* 2021;27(10):1752–1760.
900 50. Lopes MI et al. Beneficial effects of colchicine for moderate to severe COVID-19: a
901 randomised, double-blinded, placebo-controlled clinical trial. *RMD open* 2021;7(1).
902 51. Remap-Cap Investigators. Interleukin-6 Receptor Antagonists in Critically Ill
903 Patients with Covid-19. *N. Engl. J. Med.* 2021;384(16):1491–1502.
904 52. Holter JC et al. Systemic complement activation is associated with respiratory
905 failure in COVID-19 hospitalized patients. *Proc. Natl. Acad. Sci. U. S. A.*
906 2020;117(40):25018–25025.
907 53. Prendecki M et al. Temporal changes in complement activation in haemodialysis
908 patients with COVID-19 as a predictor of disease progression. *Clin. Kidney J.*
909 2020;13(5):889–896.
910 54. Cugno M et al. Complement activation and endothelial perturbation parallel
911 COVID-19 severity and activity. *J. Autoimmun.* 2021;116.
912 55. Leatherdale A et al. Persistently elevated complement alternative pathway
913 biomarkers in COVID-19 correlate with hypoxemia and predict in-hospital mortality.
914 *Med. Microbiol. Immunol.* 2022;211(1):37–48.
915 56. Siggins MK et al. Alternative pathway dysregulation in tissues drives sustained
916 complement activation and predicts outcome across the disease course in COVID-19.
917 *Immunology* 2023;168(3):473–492.
918 57. Niederreiter J et al. Complement Activation via the Lectin and Alternative Pathway
919 in Patients With Severe COVID-19. *Front. Immunol.* 2022;13.
920 doi:10.3389/fimmu.2022.835156
921 58. Fumagalli V et al. Administration of aerosolized SARS-CoV-2 to K18-hACE2 mice
922 uncouples respiratory infection from fatal neuroinvasion. *Sci. Immunol.*
923 2022;7(67):eabl9929.

924 59. Vidal E et al. Chronological brain lesions after SARS-CoV-2 infection in hACE2-
925 transgenic mice. *Vet. Pathol.* [published online ahead of print: 2021]
926 60. Kumari P et al. Neuroinvasion and Encephalitis Following Intranasal Inoculation of
927 SARS-CoV-2 in K18-hACE2 Mice. *Viruses* 2021;13(1).
928 61. Posch W et al. C5aR inhibition of nonimmune cells suppresses inflammation and
929 maintains epithelial integrity in SARS-CoV-2-infected primary human airway epithelia.
930 *J. Allergy Clin. Immunol.* 2021;147(6):2083-2097.e6.
931 62. Aiello S et al. C5a and C5aR1 are key drivers of microvascular platelet aggregation
932 in clinical entities spanning from aHUS to COVID-19. *Blood Adv.* 2022;6(3):866–881.
933 63. Crunfli F et al. Morphological, cellular, and molecular basis of brain infection in
934 COVID-19 patients. *Proc. Natl. Acad. Sci. U. S. A.* 2022;119(35):e2200960119.
935 64. Jiang Y et al. MERS-CoV infection causes brain damage in human DPP4-transgenic
936 mice through complement-mediated inflammation. *J. Gen. Virol.* 2021;102(10).
937 65. Maucourant C et al. Natural killer cell immunotypes related to COVID-19 disease
938 severity. *Sci. Immunol.* 2020;5(50).
939 66. Denk S et al. Complement C5a Functions as a Master Switch for the pH Balance in
940 Neutrophils Exerting Fundamental Immunometabolic Effects. *J. Immunol.*
941 2017;198(12):4846–4854.
942 67. Ward PA. The dark side of C5a in sepsis. *Nat. Rev. Immunol.* 2004;4(2):133–142.
943 68. Gerard NP, Gerard C. Molecular cloning of the human neurokinin-2 receptor cDNA
944 by polymerase chain reaction and isolation of the gene [Internet]. *Ann. N. Y. Acad. Sci.*
945 1991;632(1):389–390.
946 69. Gerard C. Complement C5a in the sepsis syndrome--too much of a good thing?. *N.*
947 *Engl. J. Med.* 2003;348(2):167–169.
948 70. Sadik CD, Kim ND, Iwakura Y, Luster AD. Neutrophils orchestrate their own
949 recruitment in murine arthritis through C5aR and FcγR signaling. *Proc. Natl. Acad. Sci.*
950 *U. S. A.* 2012;109(46).
951 71. Miyabe Y et al. Complement C5a Receptor is the Key Initiator of Neutrophil
952 Adhesion Igniting Immune Complex-induced Arthritis. *Sci. Immunol.* 2017;2(7).
953 72. Schmidt T et al. CD66b Overexpression and Loss of C5a Receptors as Surface
954 Markers for Staphylococcus aureus-Induced Neutrophil Dysfunction. *PLoS One*
955 2015;10(7).
956 73. Hair PS et al. Complement effectors, C5a and C3a, in cystic fibrosis lung fluid
957 correlate with disease severity. *PLoS One* 2017;12(3).

958 74. Barnes BJ et al. Targeting potential drivers of COVID-19: Neutrophil extracellular
959 traps. *J. Exp. Med.* 2020;217(6).
960 75. Zuo Y et al. Neutrophil extracellular traps in COVID-19. *JCI insight* 2020;5(11).
961 76. Middleton EA et al. Neutrophil extracellular traps contribute to immunothrombosis
962 in COVID-19 acute respiratory distress syndrome. *Blood* 2020;136(10):1169–1179.
963 77. Skendros P et al. Complement and tissue factor-enriched neutrophil extracellular
964 traps are key drivers in COVID-19 immunothrombosis. *J. Clin. Invest.*
965 2020;130(11):6151–6157.
966 78. McCubbrey AL, Allison KC, Lee-Sherick AB, Jakubzick C V, Janssen WJ.
967 Promoter Specificity and Efficacy in Conditional and Inducible Transgenic Targeting of
968 Lung Macrophages. *Front. Immunol.* 2017;8(NOV).
969 79. Dömer D, Walther T, Möller S, Behnen M, Laskay T. Neutrophil Extracellular
970 Traps Activate Proinflammatory Functions of Human Neutrophils. *Front. Immunol.*
971 2021;12. doi:10.3389/fimmu.2021.636954
972 80. Nakazawa D et al. The responses of macrophages in interaction with neutrophils
973 that undergo NETosis. *J. Autoimmun.* 2016;67:19–28.
974 81. Lee YH, Giraud J, Davis RJ, White MF. c-Jun N-terminal kinase (JNK) mediates
975 feedback inhibition of the insulin signaling cascade.. *J. Biol. Chem.* 2003;278(5):2896–
976 902.
977 82. Hoenigl M et al. The emergence of COVID-19 associated mucormycosis: a review
978 of cases from 18 countries. *The Lancet. Microbe* [published online ahead of print:
979 2022].
980 83. Grasselli G, Cattaneo E, Florio G. Secondary infections in critically ill patients with
981 COVID-19. *Crit. Care* 2021;25(1).
982 84. Kooistra EJ et al. Dexamethasone and tocilizumab treatment considerably reduces
983 the value of C-reactive protein and procalcitonin to detect secondary bacterial infections
984 in COVID-19 patients. *Crit. Care* 2021;25(1).
985 85. Rothe K et al. Dexamethasone therapy and rates of secondary pulmonary and
986 bloodstream infections in critically ill COVID-19 patients. *Multidiscip. Respir. Med.*
987 2021;16(1):162–169.
988 86. Crew PE et al. Disseminated Gonococcal Infections in Patients Receiving
989 Eculizumab: A Case Series. *Clin. Infect. Dis.* 2019;69(4):596–600.
990 87. Langereis JD et al. Eculizumab impairs Neisseria meningitidis serogroup B killing
991 in whole blood despite 4CMenB vaccination of PNH patients. *Blood Adv.*

2020;4(15):3615–3620.
88. Xu R et al. Complement 5a receptor-mediated neutrophil dysfunction is associated with a poor outcome in sepsis. *Cell. Mol. Immunol.* 2016;13(1):103–109.
89. Fattahi F, Zetoune FS, Ward PA. Complement as a Major Inducer of Harmful Events in Infectious Sepsis. *Shock* 2020;54(5):595–605.
90. Rittirsch D et al. Functional roles for C5a receptors in sepsis. *Nat. Med.* 2008;14(5):551–557.
91. Herrmann JB et al. Complement c5a receptor 1 exacerbates the pathophysiology of n. Meningitidis sepsis and is a potential target for disease treatment. *MBio* 2018;9(1).
92. Karsten CM et al. Monitoring and cell-specific deletion of C5aR1 using a novel floxed GFP-C5aR1 reporter knock-in mouse [Internet]. *J. Immunol.* 2015;194(4):1841–1855.
93. Duarte-Neto AN et al. Pulmonary and systemic involvement in COVID-19 patients assessed with ultrasound-guided minimally invasive autopsy. *Histopathology* 2020;77(2):186–197.

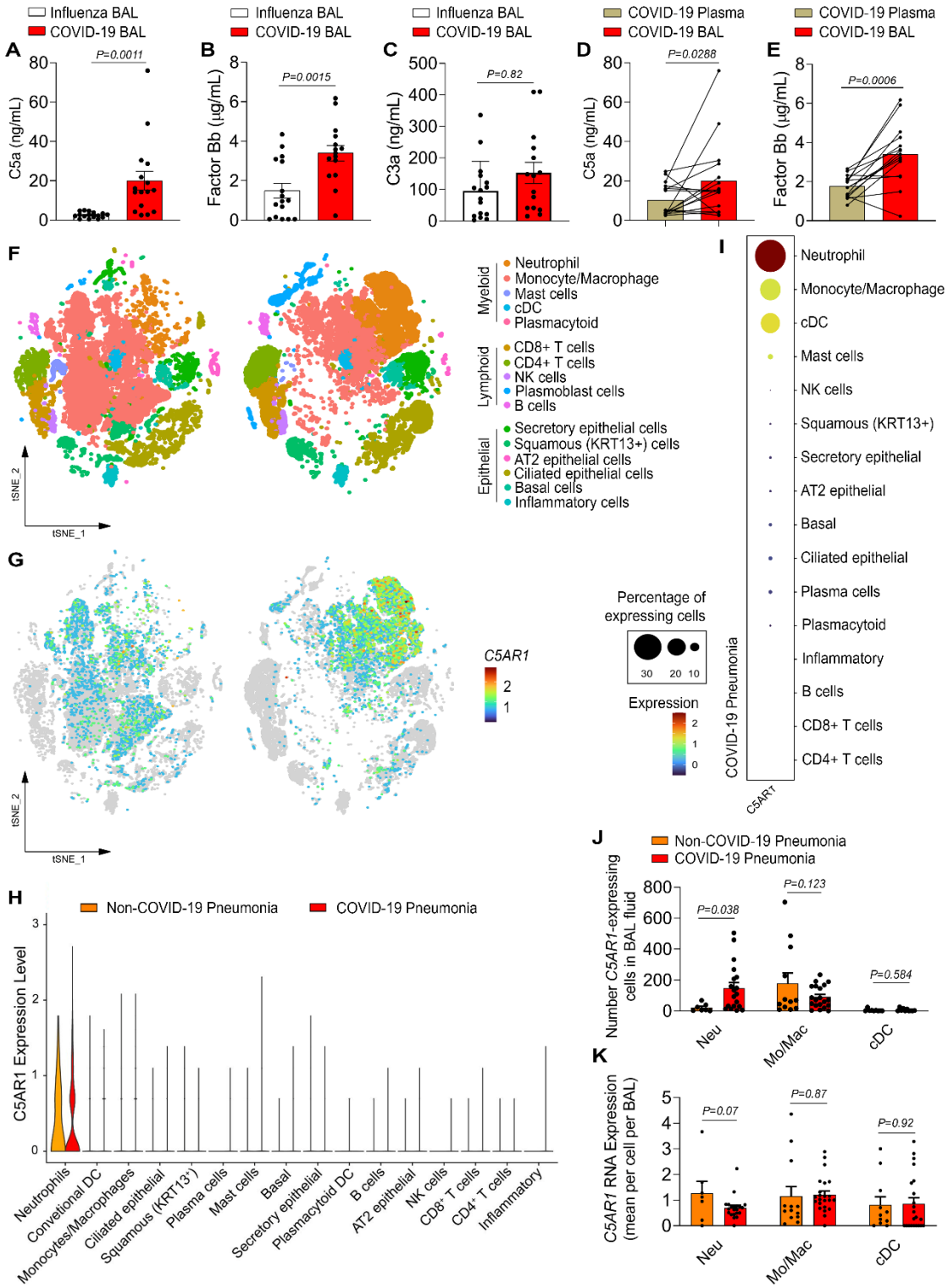

Figure 1 – C5a levels and *C5AR1* expression in the BAL fluid and cells from COVID-19 patients. An ELISA assay was performed to measure the concentrations of (**A**) C5a, (**B**) factor Bb, and (**C**) C3a in the BAL fluid from non-COVID-19 (n=16) and COVID-19 patients (n=16). (**B**) Paired concentrations of (**D**) C5a and (**E**) factor Bb in the plasma and BAL fluid from COVID-19 patients were determined by ELISA. (**F**) A different cohort from a previously published dataset was re-analyzed and the t-Distributed

Stochastic Neighbor Embedding (t-SNE) analysis of total cells (65,166) from BAL fluid of non-COVID-19 pneumonia (n=13) and COVID-19 patients (n=22) is shown. (**G**) Dot plots display the highlighted distribution of *C5AR1* for each indicated cell population. (**H**) Violin plots showing the expression levels of *C5aR1* in each type of cell from COVID-19 or non-COVID-19 patients. (**I**) The dot plot depicts the scaled and centered expression of an average cell in each cluster and therefore contains negative and positive values. The average expression reflects the mean expression of *C5AR1* in each cluster compared with all other cells. (**J**) Number of cells per cell population [neutrophils (Neu), monocytes/macrophages (Mo/Mac), and dendritic cells (cDC)] that express *C5AR1* in the groups COVID-19 and non-COVID-19. (**K**) Average expression of *C5AR1* per cell for each cell population [neutrophils (Neu), monocytes/macrophages (Mo/Mac), and dendritic cells (cDC)] in the groups COVID-19 and non-COVID-19. Data are shown as the mean ± SEM. P values were determined by two-tailed unpaired (**A - D, and J and K**) or paired (**D and E**) Student *t*-test followed by Wilcoxon matched-pairs signed rank test.

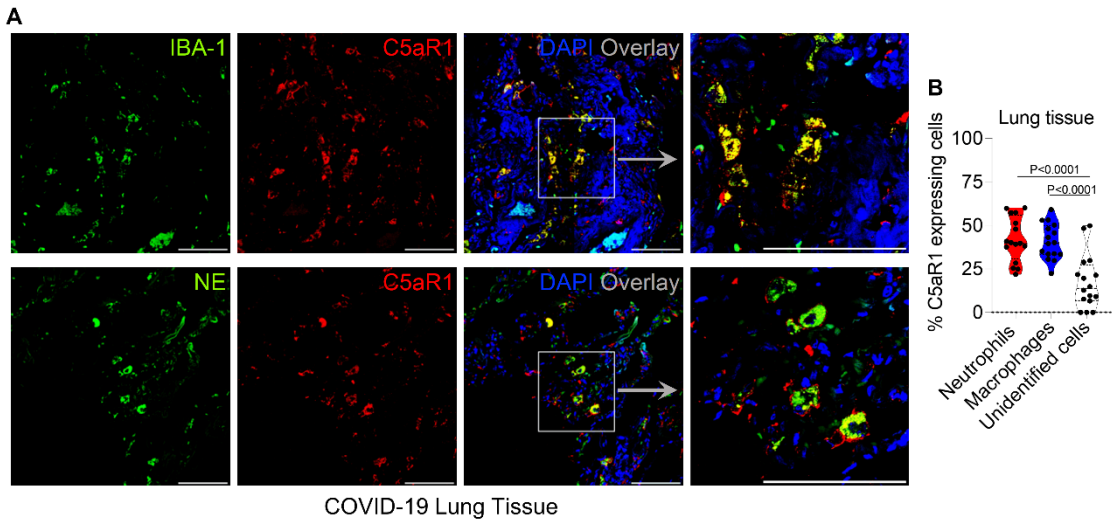

Figure 2 – C5aR1 is expressed in macrophage and neutrophil in the lung tissue of COVID-19 patients. (**A**) Representative confocal images of the presence of C5aR1 in macrophage (Iba-1) and neutrophil (neutrophil elastase, NE) in the lung tissue from autopsies of COVID-19 patients (n=4 cases/4 randomized field). Cells were stained for nuclei (DAPI, blue), Iba-1 or NE (green), and C5aR1 (red). Scale bar indicates 50 µm. (**B**) Percentage of cells expressing C5aR1 in the COVID-19 lung. Data are shown as the mean ± SEM. P values were determined by ANOVA followed by Bonferroni's post hoc test (**B**).

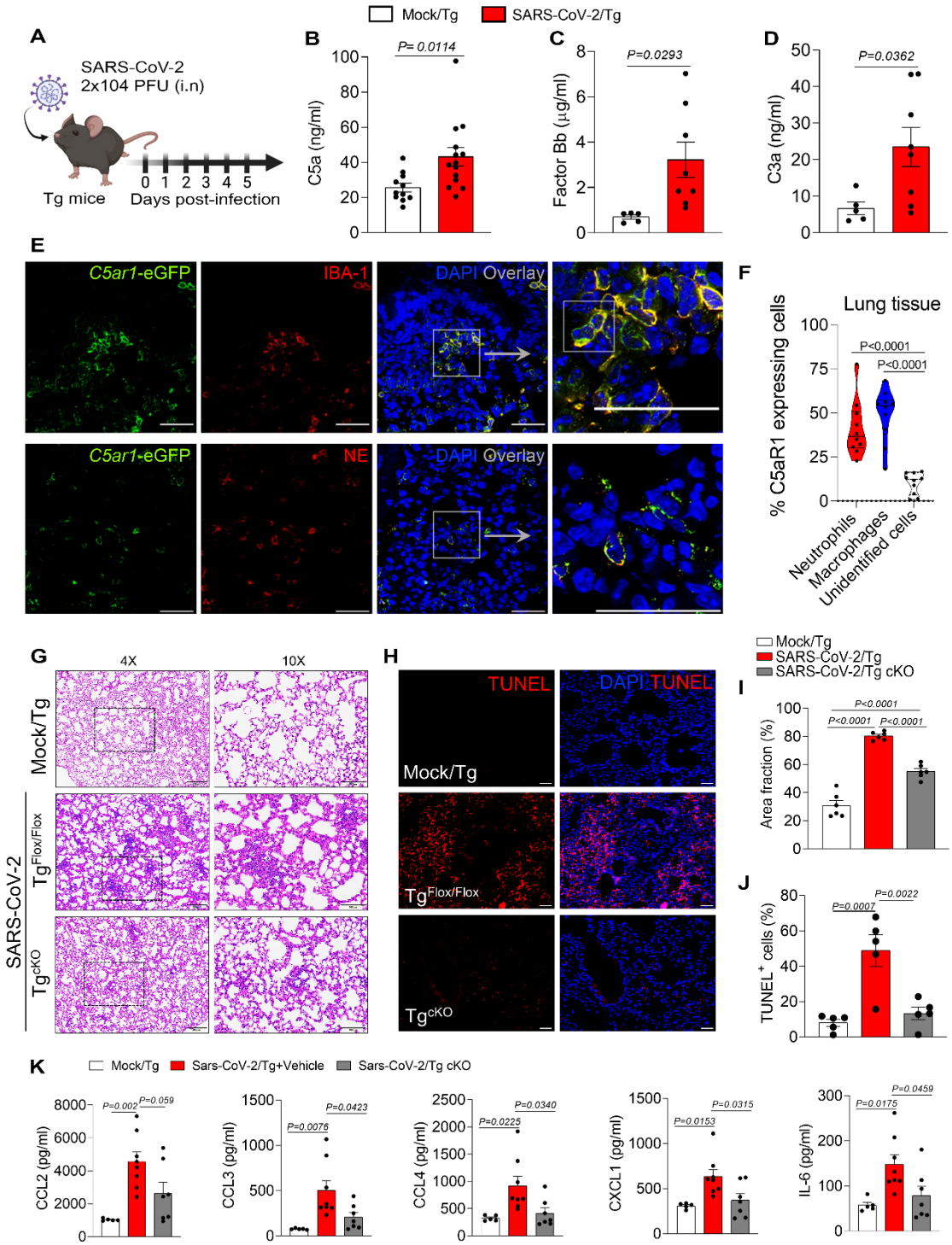

Figure 3 - C5aR1 signaling on myeloid cells contributes to the lung pathology in a COVID-19 mouse model. (**A**) Tg mice were infected with SARS-CoV-2 (2 x 10^4 PFU, i.n). ELISA assay to measure levels of (**B**) C5a in the lung homogenate of infected animals (n=14) or mock control (n=11). (**C**) factor Bb and (**D**) C3a levels in the lung homogenate of infected animals (n=8) or mock control (n=5). (**E**) Representative confocal images of the presence of C5aR1 expression in the lung tissue of $Tg^{Flox/Flox}$ mice (*C5ar1*-eGFP mice) infected with SARS-CoV-2 (5 dpi). Tissue slices were co-stained for

nuclei (DAPI, blue), Iba-1 (macrophages, red) and NE (neutrophils, red) markers. Scale bar indicates 50 µm. (**F**) Percentage of cells expressing C5aR1 in the lung tissue of $Tg^{Flox/Flox}$ mice infected with SARS-CoV-2 (n=4 mice/4 randomized field). (**G**) Representative H&E staining from the lung of SARS-CoV-2-infected $Tg^{Flox/Flox}$ (n=6) or Tg^{cKO} mice (n=6). Mock was used as control (n=6). Scale bars - 4X: 200 µm, 10X: 100 µm. (**H**) TUNEL staining (red) for detection of apoptotic cells in situ from lung tissue of SARS-CoV-2-infected TgFlox/Flox (n=5) or TgcKO mice (n=6). Mock-infected Tg mice were used as a control (n=5/group). (**I**) Quantification of the lung septal area fraction. (**J**) Percentage of TUNEL positive cells in lung tissue. Scale bar indicates 50 µm. (**K**) ELISA assays were performed to detect CCL2, CCL3, CCL4, CXCL1 and IL-6 levels in the lung tissue of $Tg^{Flox/Flox}$ (n=8) or Tg^{cKO}-infected mice (n=7). Mock-infected Tg mice were used as a control (n=5). Data are shown as the mean ± S.E.M. P values were determined by (**B - D**) Student' *t*-test and (**F, I, J and K**) one-way ANOVA followed by Bonferroni's post hoc test.

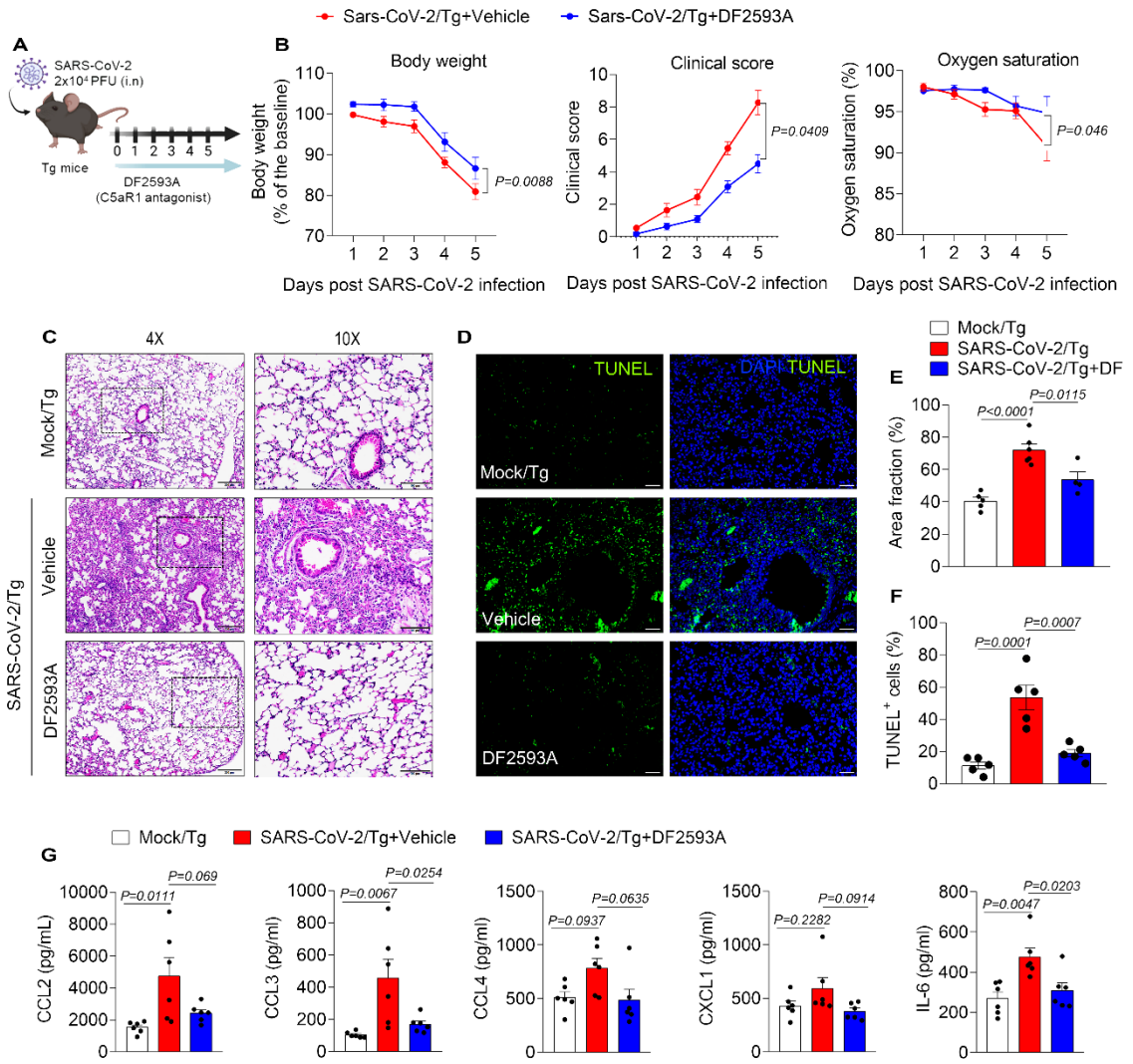

Figure 4 – DF2593A, a selective C5aR1 antagonist, ameliorates COVID-19 in mice model. (**A**) Tg mice were infected with SARS-CoV-2 (2 x 10^4 PFU, i.n) and treated with DF2593A (3 mg/kg, p.o) 1 h before SARS-CoV-2 infection and once a day up to the day of sample collection (5 dpi). (**B**) Body weight, clinical score, and oxygen saturation were measured daily post-infection (n=11/group, pooled from 2 independent experiments). (**C**) Representative H&E staining from the harvested lung of the COVID-19 mouse model treated (n=4) or not (n=6) with DF2593A. Mock was used as control (n=5). Scale bars - 4X: 200 µm, 10X: 100 µm. (**D**) TUNEL staining (green) for detection of apoptotic cells in situ from lung tissue of mice (n=5/group). (**E**) Quantification of the lung septal area fraction. (**F**) Percentage of TUNEL positive cells in lung tissue. Scale bar indicates 50 µm. (**G**) ELISA assays were performed to detect CCL2, CCL3, CCL4, CXCL1 and IL-6 levels in lung homogenate (n=6/group). Mock was used as the control group. Data are shown as the mean ± S.E.M. P values were determined by one-way ANOVA followed by Bonferroni's post hoc test (**E, F and G**).

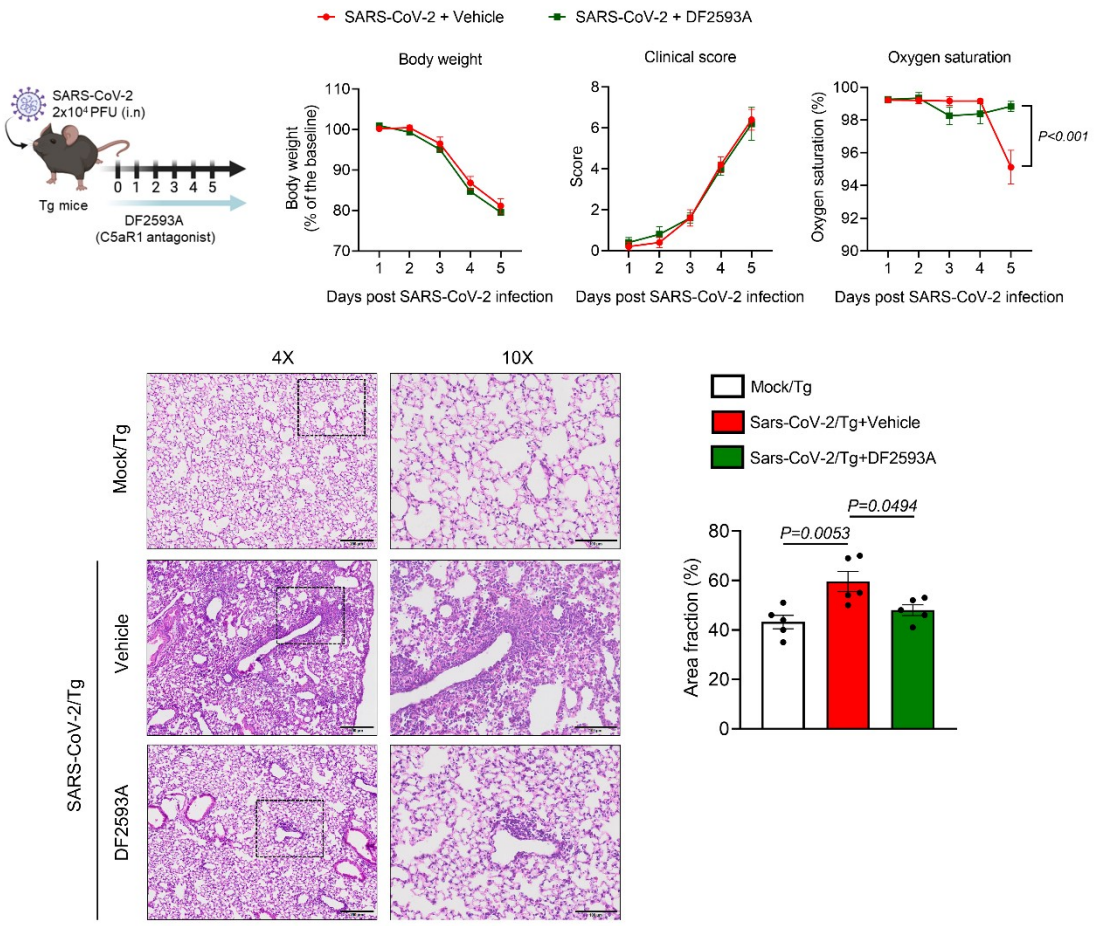

Figure 5 – The post-infection treatment with DF2593A reduced lung pathology/disfunction in SARS-CoV-2-infected Tg mice. (**A**) Tg mice were infected with SARS-CoV-2 (2 x 10^4 PFU, i.n) and treated with DF2593A (3 mg/kg, p.o) 24 h after SARS-CoV-2 infection and once a day up to the day of sample collection (5 dpi). (**B**) Body weight, clinical score, and oxygen saturation were measured daily post-infection (n=5/group). (**C**) Representative H&E staining from the harvested lung of the COVID-19 mouse model treated or not with DF2593A (n=5/group). Mock was used as control (n=5). Scale bars - 4X: 200 µm, 10X: 100 µm. (**E**) Quantification of the lung septal area fraction. Data are shown as the mean ± S.E.M. P values were determined by one-way ANOVA followed by Bonferroni's post hoc test (**D**).

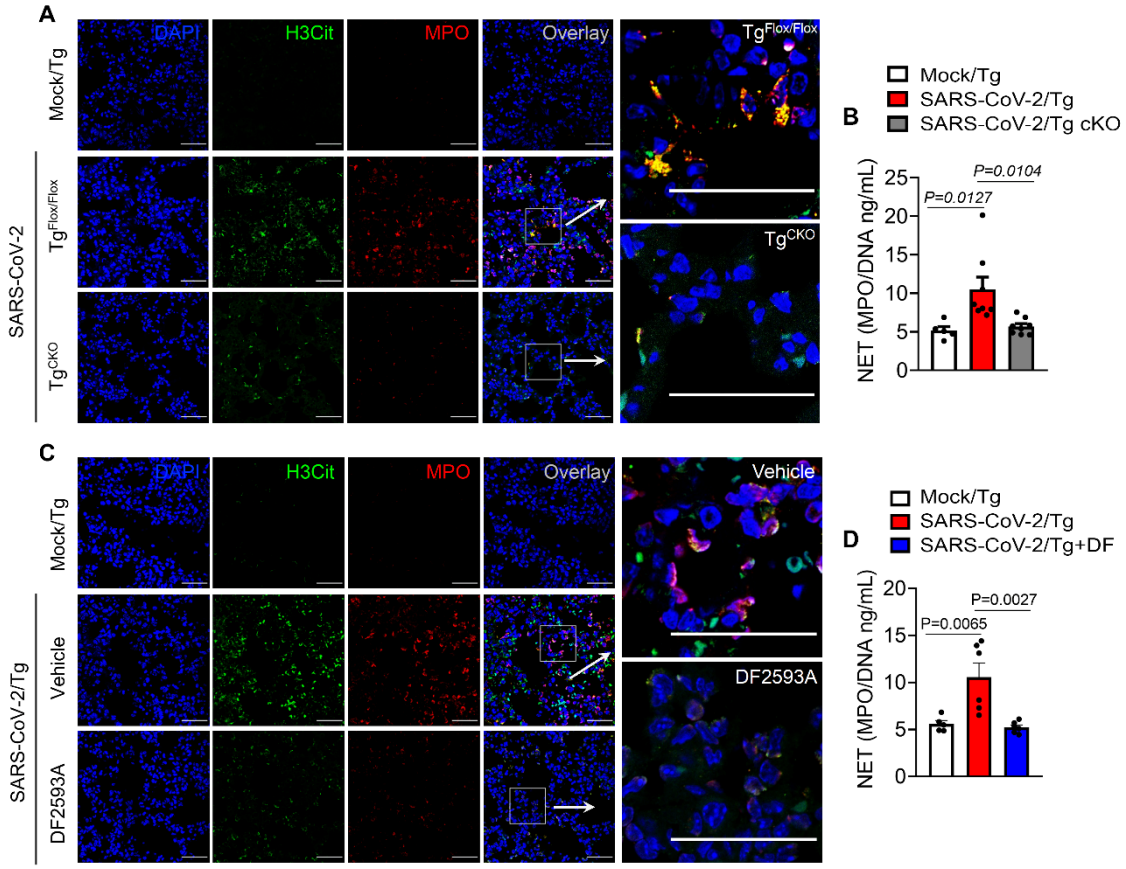

Figure 6 - C5a/C5aR1 signaling is involved in the pathophysiology of COVID-19 through NET formation. $Tg^{Flox/Flox}$ (n=8) and Tg^{cKO} (n=8) mice were infected with SARS-CoV-2 (2 x 10^4 PFU, i.n). (**A**) Representative confocal images showing the presence of NETs in the lung tissue from $Tg^{Flox/Flox}$ or Tg^{cKO}-infected mice. A mock-infected group was performed as control (n=5). Staining shows nuclei (DAPI, blue), H3Cit (green), and myeloperoxidase (MPO) (red). (**B**) At 5 dpi, the levels of NETs were quantified by MPO-DNA PicoGreen assay in the supernatant of the lung homogenate. (**C**) Tg-infected mice were treated with DF2593A (3mg/kg, p.o, n=6) or vehicle (n=5/group). Representative confocal images showing the presence of NETs in the lung tissue of Tg-infected mice treated with DF2593A or vehicle (n=5/group). Mock-infected group was performed as control (n=5). (**D**) At 5 dpi, NETs levels were quantified by MPO-DNA PicoGreen assay in the supernatant of the lung homogenate. Data are shown as the mean ± S.E.M. P values were determined by one-way ANOVA followed by Bonferroni's post hoc test (**B and D**). Scale bar indicates 50 µm.

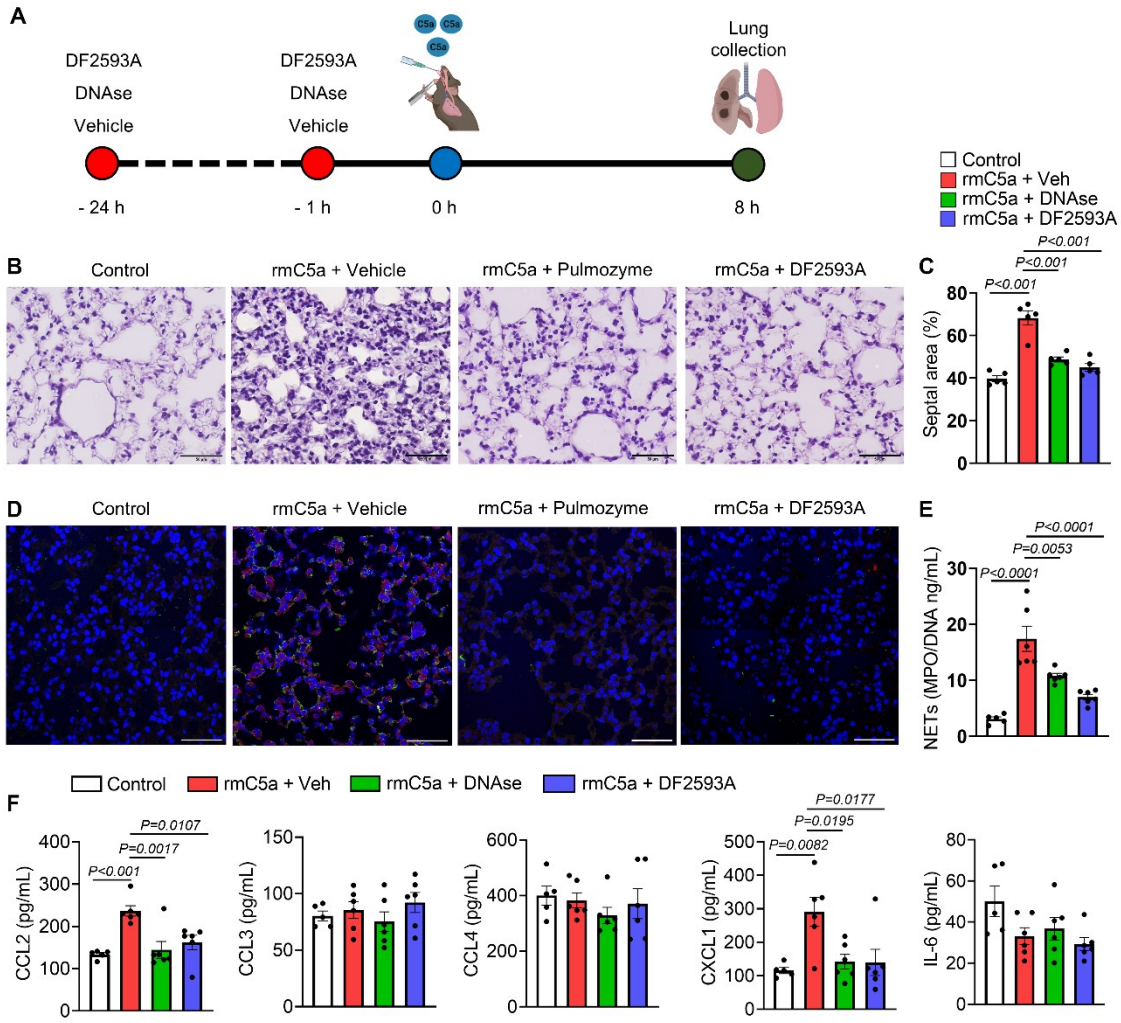

Figure 7 – Intratracheal instillation with C5a induced lung immunopathology via C5aR1 signaling and NETs (**A**) C57/BL6 mice were treated twice with vehicle, DNAse (Pulmozyme®, 10 mg/kg, s.c.), or C5aR1 antagonist (DF2593A, 3 mg/kg, p.o.), 24 h and 1 h before the intratracheal instillation of rmC5a (400 ng), and the lungs were harvested and processed for H&E staining (n=5/group). (**B**) Quantification of the lung septal area fraction. (**C**) Lung slices from the control group or from mice challenged with rmC5a and treated with vehicle, DNAse, or C5aR1 antagonist (DF2593A) were co-stained for nuclei (DAPI, blue), H3Cit (green) and MPO (red) markers. (**D**) NET quantification by the MPO-DNA PicoGreen assay in the supernatant of the lung homogenate (n=5-6/group). (**E**) ELISA assays were performed to detect CCL2, CCL3, CCL4, CXCL1 and IL-6 levels in lung homogenate (n=5-6/group). Data are shown as the mean ± S.E.M. P values were determined by one-way ANOVA followed by Bonferroni's post hoc test (**B and D**).

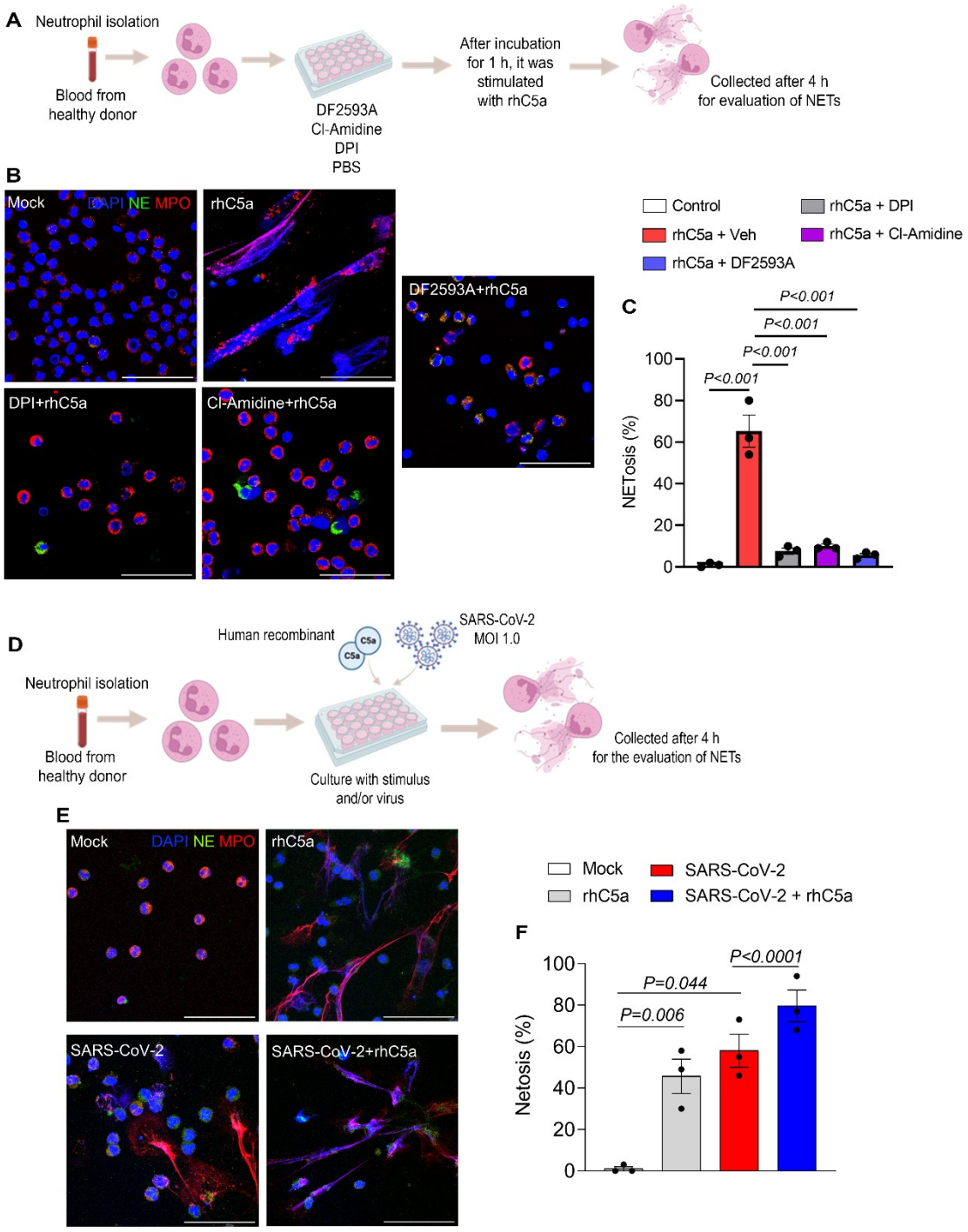

Figure 8 - C5a is able to directly promote and enhance SARS-CoV-2-induced NETosis (**A**) Isolated human neutrophils were incubated with PBS, DPI, Cl-amidine, or DF2593A for 1 h and then challenged with rhC5a (3 nM) for 4 h. (**B**) Cells were stained for nuclei (DAPI, blue), NE (green), and MPO (red). (**C**) Percentage of NETs quantification in these neutrophils supernatants (n=3 donors). (**D**) Neutrophils were isolated from healthy donors and incubated with mock, rhC5a (3 nM) and SARS-CoV-2 (MOI = 1.0) for 4 h. One group of SARS-CoV-2-infected cells was pretreated with rhC5a

(3 nM). (**E**) Representative images of NETs release. Cells were stained for nuclei (DAPI, blue), NE (green), and MPO (red). The scale bar indicates 50 μm. (**F**) Percentage of NETs quantification in these neutrophils supernatants (n=3 donors). Data are shown as the mean ± S.E.M. P values were determined by one-way ANOVA followed by Bonferroni's post hoc test (**C** and **F**).